

Numerical calculations of the thermal-aerodynamic characteristics in a solar duct with multiple V-baffles

Younes Menni ^a, Mahyar Ghazvini ^b, Houari Ameer ^c, Mohammad Hossein Ahmadi ^d,
Mohsen Sharifpur ^{e,f} and Milad Sadeghzadeh ^g

^aUnit of Research on Materials and Renewable Energies, Department of Physics, Faculty of Sciences, Abou Bekr Belkaid University, Tlemcen, Algeria; ^bDepartment of Ocean and Mechanical Engineering, Florida Atlantic University, Boca Raton, FL, USA; ^cDepartment of Technology, University Centre of Naama (Ctr Univ Naama), Naama, Algeria; ^dFaculty of Mechanical Engineering, Shahrood University of Technology, Shahrood, Iran; ^eInstitute of Research and Development, Duy Tan University, Da Nang, Viet Nam; ^fDepartment of Mechanical and Aeronautical Engineering, University of Pretoria, Pretoria, South Africa; ^gDepartment of Renewable Energy and Environmental Engineering, University of Tehran, Tehran, Iran

ABSTRACT

The study aimed to enhance the heat transport by improving the hydrodynamic structure of the system by changing and restructuring the duct's internal geometry. Modern fins, of the shape 'V', have been proposed with different dimensions, and they are periodically arranged over the duct surfaces. The most important steps of this research are the change in the V-fin attack-angle (40°–80°), length ($H_b/2$, $3H_b/4$, H_b , $5H_b/4$ and $3H_b/2$), and separation length ($D_s/2$, $3D_s/4$, D_s and $5D_s/4$), as well as the flow rate (6×10^3 – 3×10^4). The study yielded an optimum case for a 40-degree attack-angle, with a factor of thermal enhancement of 2.163 for the highest value of Reynolds number. On the other hand, improving the length of the V-fins or decreasing in the space between them, increases the flow strength by enlarging the recycling cells, which reflects on the hydrodynamic behavior, and changes the heat transfer. The presence of this new model of fins also highlights a hydrothermal improvement ranging between 1.196 and 23.779 percent compared to the previously indicated models, reflecting the effectiveness of the new system of solar heat exchangers with air V-finned ducts.

ARTICLE HISTORY

Received 18 April 2020
Accepted 21 August 2020

KEYWORDS

CFD; solar heat exchangers;
air V-finned ducts; recycling
cells; heat transfer



Nomenclature

\vec{V}	vector of velocity [m/s]
\bar{U}	average velocity of the section [m/s]
$C_{1\varepsilon}$	constant in k - ε model
$C_{2\varepsilon}$	constant in k - ε model
C_f	local coefficient of friction
C_p	specific heat [J/kg K]
C_p	coefficient of pressure
D_h	aeraulic diameter of the exchanger [m]
D_s	space between fins [m]
f	average coefficient of friction
f_0	factor of friction for smooth exchanger
G_k	rate of production for k
H_b	height of fin [m]
H_c	height of exchanger [m]
K	kinetic energy of turbulence [m^2/s^2]
k_f	thermal-conductivity of fluid [W/m K]
L	length of exchanger [m]
L_{in}	inlet-1st fin space [m]
L_{out}	4th fin -exit space [m]

Nu	average number of Nusselt
Nu_0	Nusselt number for smooth exchanger
Nu_x	local number of Nusselt
P	pressure [Pa]
Pd	dynamic pressure [Pa]
Pr	number of Prandtl
Re	number of Reynolds
T	temperature [K]
u	horizontal velocity [m/s]
U_{in}	intake velocity [m/s]
v	vertical velocity [m/s]
V	mean velocity [m/s]
w	thickness of fin [m]
W	width of exchanger [m]
ΔP	pressure drop [Pa]

Greek letter

TEF	factor of thermal performance
ε	rate of dissipation of turbulence [m^2/s^3]

CONTACT Mohammad Hossein Ahmadi  mohammadhosein.ahmadi@gmail.com; Mohsen Sharifpur  mohsen.sharifpur@up.ac.za, mohsensharifpur@duytan.edu.vn

α	angle of attack of fin [degree]
μ	dynamic viscosity [kg/m s]
μ_t	turbulent viscosity [kg/m s]
ρ	density of fluid [kg/m ³]
σ_k	constant in K -equation
σ_ε	constant in ε -equation
τ_w	wall-shear-stress [Pa]
ψ	stream-function [kg/s]

Subscript

0	smooth
a	aerualic
b	baffle
c	exchanger conduit
f	fluid
in	intake
max	maximum
out	outlet
ref	reference
s	separation
t	turbulent
x	local

Introduction

Solar energy is modern, pure, renewable, and inexhaustible (Ahmadi et al., 2020; Beyaztas et al., 2019; Samadianfard et al., 2019). Transforming solar energy into thermal energy via solar collectors is a topic of interest to many researchers (Abuşka, 2018; Kabeel et al., 2018). Solar air duct heat exchangers target many studies (Amraoui & Aliane, 2018; Hassan & Abo-Elfadl, 2018; Ho et al., 2017). The inclusion of obstacle-type vortex generators is one of the most effective and ongoing techniques to date (Ameur, 2020; Ameur & Menni, 2019; Jain et al., 2019; Kumar et al., 2018; Kumar & Kim, 2015). We present in this axis some of the numerical and experimental studies that have become popular in this field, starting with researchers Promvonge and Thianpong (2008). Some experiments have been carried out by these authors for evaluating friction loss and turbulent forced-convective heat transfer of airflow within a steady heat flux channel equipped with different-configurations ribs. The structures of the ribs were rectangular, wedge, and triangular. The study showed an increase in the value of Nusselt number as well as in the coefficient of skin friction in the case of a wedge-section rib, while the highest thermal performance was recorded in the case of a triangular-geometry rib with a staggered arrangement. Furthermore, convective transfer of heat, as well as laminar fluid flow attributes in a 2-D horizontal channel

with adding diamond-shaped baffles under the condition of isothermal walls have been numerically studied by Sripattanapipat and Promvonge (2009). In this study, outcomes of distinct baffle tip angles on pressure loss as well as thermal performance within the channel have been evaluated, and comparisons of using flat and diamond baffles have been provided. A comparison of different diamond baffles showed high thermal performance for the attack angle of 5 degrees, while the flat baffle showed a decrease in the same factor and for all Reynolds values followed, compared to the diamond baffle with an angle of attack varying from 5 to 10 degrees. In another study, hydrodynamic behavior was detected as well as an examination of heat transfer in a rectangular structure of a channel equipped with pin-typed fins (Wang et al., 2012). Also, the comparison of various shaped pin fins with identical cross-sectional areas such as drop-shaped, elliptical, and circular in a staggered arrangement has been presented. The results showed an improvement in the thermal performance in the case of circular-type pins compared to the case of drop-geometry pins.

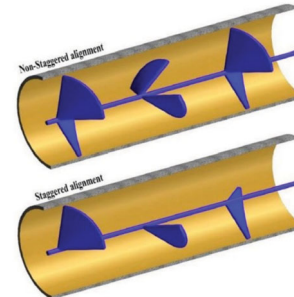
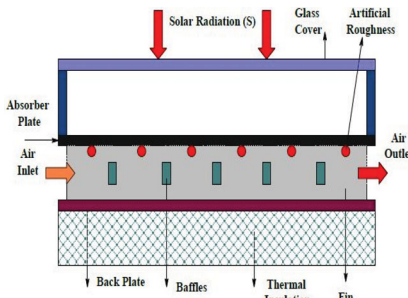
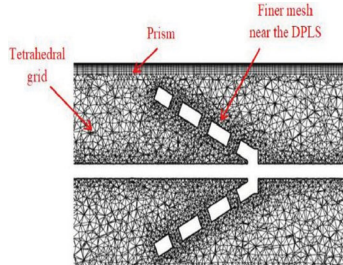
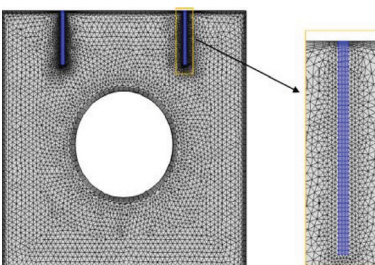

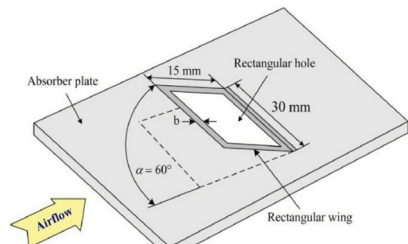
Furthermore, Reddy and Satyanarayana (2008) performed a 3-D CFD simulation of a new solar receiver for the aim of improving thermal performance. The receiver contained different porous inserts like circular, trapezoidal, and square shapes. The comparative results showed that the trapezoidal-shape porous-type inserts increase the heat transfer by about 13.8% in the case of 1.7 kPa of pressure penalty and 6.4 kg/s of fluid mass. Using the FLO EFD 9.0 type CFD software, Xu et al. (2014) conducted a detailed numerical analysis of the flow fields as well as the isotherms in a computer board. The whole system adopted the combination of liquid-type cooling and air-type cooling to increase heat transfer. The computational results showed an improvement in the heat dissipation efficiency in the presence of fin-type heat sinks, as the temperature of the CPU case dropped from 186° to 149°C. Also, Jayavel and Tiwari (2010) used a 3D CFD code to address the hydrothermal characteristics through a rectangular-configuration channel by using the tube separation technique. Their results reported that the heat transfer could be enhanced in both cases of the tube arrangement, i.e. in-line and staggered, by reducing the separation length between them. Vatani and Mohammed (2013) applied various rib-groove structures such as arc, square, and triangles with different nanofluids containing SiO₂, ZnO, CuO, Al₂O₃ to numerically investigate hydraulic and thermal characteristics of flow in the channel. As indicated in the results, the greatest Nusselt number can be achieved by using SiO₂/water nanofluid among all the nanofluids. Moreover, in another CFD study, different rib orientations have been used by Gao et al. (2018) with the

aim of improving the heat transfer in a U-duct when $Re = 3 \times 10^4$. The study showed that the recirculation core technique is an important visualization way for flow checking and optimization in U-section cooling-type ducts with angled-geometry ribs. Also, Cao et al. (2019) conducted a study by using experimental techniques as well as numerical schemes on a new heat exchanger model with inserting sextant helical baffle for the aim of improving thermal performance. The analysis of comparison results revealed that the efficiency of the sextant-type scheme is greater than that of the quadrant one. In addition, the authors indicated that this study can be adopted as a theoretical database for updating heat exchangers according to new models.

Saini and Saini (2008) conducted a study by using experimental methods for developing the transfer of heat in a solar heater with airflow and arc-shape parallel wire to increase roughness. Furthermore, they investigated the friction factor augmentation caused by these elements. Their study obtained a maximum thermal improvement of about 3.8 times for the relative angle of the wire estimated at 0.3333 with a relative height of 0.0422. This improvement also corresponds to an increase in the factor of friction, as it was estimated by about 1.75 times at the same previous dimensions. Skullong et al. (2014) conducted a study by using experimental methods for investigating thermal performance and airflow characteristics into a great solar heater duct given by groove-type turbulators and wavy-type ribs. Their study showed an enhancement in the Nusselt number and friction coefficient for the case of simultaneous use of rib-groove on both duct surfaces compared to the smooth-type duct in the presence or absence of ribs. Also, an innovative method to improve the transfer of heat and decrease friction-loss inside a heat exchanger provided by circular-type tubes have been introduced by Torii et al. (2002) using turbulators of winglet-type. The results reveal that there is a 30% increase in heat transfer in the case of overlapping tube banks, while it is 20% in the inline-manner tube bank second case. In another study, an experimental comparison was made by Zhou and Ye (2012) between conventional winglet-type vortex generators, i.e. delta, rectangular and trapezoidal, with novel winglet-type vortex generators, i.e. curved trapezoidal. The results concluded with the selection of the traditional model of vortex generators with a delta-type winglet for laminar flows as well as transitional streams, while the effectiveness of the new winglet model of curved trapezoidal type was confirmed for completely turbulent flows. Additionally, an especial flow layout has been designed by Du et al. (2017) to check the molten salt performance for heat transfer in a heat exchanger fitted with fractional obstacles in Reynolds numbers between 6,142 and 9,125 and

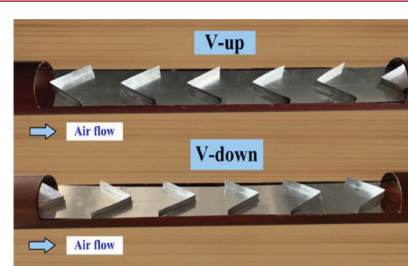

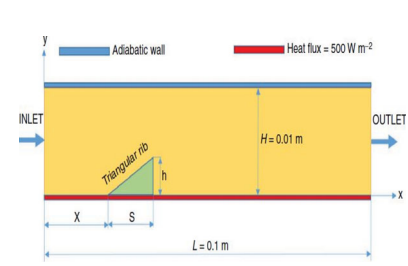
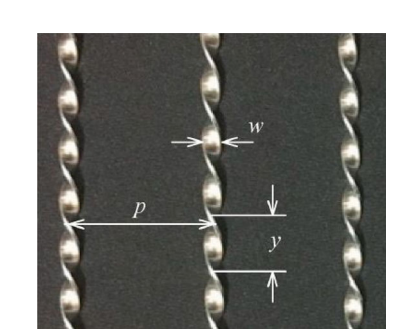
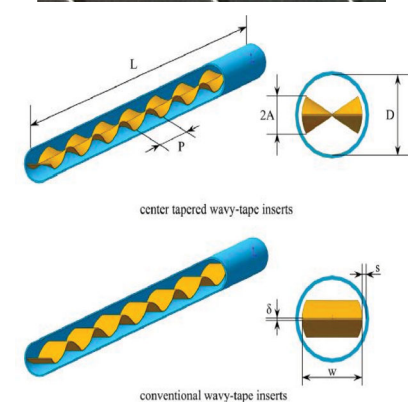
high temperature. The authors reported an increase of 26% in values of Nusselt number, in the cases of using segmental obstacles and molten salt for a low stream rate. Lei et al. (2008) simulated by using numerical approaches the effectiveness of the attack value of helical-form baffles on the performance of heat exchangers. According to the results, the mean Nusselt number is augmented by increasing the baffle inclination. Additionally, Wen et al. (2015) developed a pattern of a ladder-type baffle for the purpose of enhancing the thermal performance of heat exchangers by utilizing helical baffles. The results confirmed the importance of using the foldable ladder-model of helical baffles to enhance thermal performance in such heat exchangers used. Also, an experiment has been conducted by Bopche and Tandale (2009) to study skin friction and convective coefficient of heat transfer in the solar duct from an air heater by inserting U-shaped turbulators. The study showed an augmentation of about 2.82 times in terms of heat transfer, while 3.72 times in terms of friction, compared to the smooth-wall duct. Basing on experimental approaches, Promvong et al. (2015) evaluated the influences of width ratios and pitch length for horseshoe-type turbulators with 20° inclination on the hydrothermal aspects of a tubular section heat exchanger. As indicated in the results, the heat transfer rate improved significantly. Skullong et al. (2016) reported a computational and applied study in order to collect the impacts of using 30° horseshoe-baffle (HB) in a square duct on thermal performance and turbulent flow. Comparing the performance of using these HBs, it turns out that there is a high improvement received from this horseshoe-type new model, much better than in the case of the presence of wire coils. Also, Singh et al. (2011) used experimental methods to determine the effects of using discrete V-down rib in a rectangular duct on the fluid flow as well as the thermal characteristics with consistent heat flux. Their study concluded to demonstrate the effectiveness of the new baffle structure, which gave an increase in Nusselt number by about 3.04 folds and an augmentation in skin friction by about 3.11 times relative to the smooth-wall duct. Boonloi and Jedsadaratanachai (2016) numerically investigated thermal performance enhancement of a square-geometry duct containing discrete-section combined-model vortex generators. In their simulation, the effects of flow directions and blockage ratios in a turbulent regime, i.e. $3,000 < Re < 20,000$, have been analyzed. Under the conditions used, the thermal transfer enhancement has been updated about 2.8 to 6 times if compared to the results of the smooth-walled channel. Furthermore, an experiment has been carried out by Chamoli and Thakur (2016) with the purpose of determining friction factor along with the thermal characteristics in a rectangular

Table 1. New physical domain with novel vortex generators.

Author (s)	Physical model	Physical domain
Pourramezan et al. (2020)	<ul style="list-style-type: none"> - Circular type tube with twisted-conical-strip form inserts - Laminar flow - Taguchi approach - ANSYS Fluent 14.5 	
Saravanakumar et al. (2020)	<ul style="list-style-type: none"> - Air heater with arc-type ribs - Extended-type surface - Exergetic analysis - Optimization - MATLAB 	
Nakhchi et al. (2020)	<ul style="list-style-type: none"> - Heat exchangers with perforated-louvered-strip type inserts - $Re = 5,000-14,000$ - RNG type $k-\epsilon$ - Ansys ICEM CFD 18.1 	
Saleh et al. (2019)	<ul style="list-style-type: none"> - Square-form enclosure with 2 elastic-type fins - Laminar flow - Mixed-convection - Arbitrary Lagrangian-Eulerian 	
Yu et al. (2020)	<ul style="list-style-type: none"> - Shell and tube type HE with longitudinal VGs - Turbulent flow - RSM numerical study 	
Promvong and Skullong (2019a)	<ul style="list-style-type: none"> - Solar receiver with hole punched type wings - Heat transfer - Turbulent flow - $Re = 5,300-22,600$ - Experimental study 	

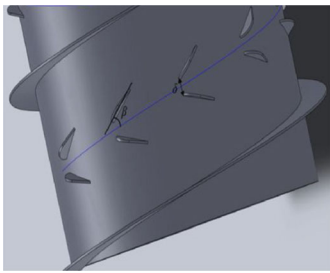
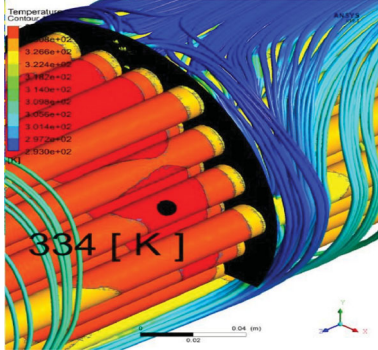
(continued)

Table 1. Continued.

Author (s)	Physical model	Physical domain
Promvonge and Skullong (2020)	<ul style="list-style-type: none"> - Tubular type HE with - V-baffled type tapes - Forced convection - $Re = 4,120-25,800$ - ANSYS Fluent 	
Promvonge and Skullong (2019b)	<ul style="list-style-type: none"> - Solar receiver with combined turbulators - Forced-convection - Turbulent flow - $Re = 5,300-23,000$ - Experimental study 	
Ekiciler (2020)	<ul style="list-style-type: none"> - Duct with triangular-type rib - Hybrid nanofluid - Turbulent flow - $Re = 50,000-100,000$ - Finite volume - RNG type $k-\epsilon$ 	
Eiamsa-ard and Chuwattanakul (2020)	<ul style="list-style-type: none"> - Channels with - Twisted type baffles - Heat transfer - $Re = 4,000-20,000$ - Heat transfer - Experimental study 	
Liang et al. (2019)	<ul style="list-style-type: none"> - Tubes with inserts - Water type fluid. - Heat transfer - Laminar flow - $Re = 6,00-1,800$ - Numerical study - Finite volume - FLUENT 14.0 	

(continued)

Table 1. Continued.

Author (s)	Physical model	Physical domain
Zhang et al. (2019)	<ul style="list-style-type: none"> - Helical type channel with VGs - Experimental study - 3D simulation - SIMPLE-algorithm - ANSYS FLUENT 	
Biçer et al. (2020)	<ul style="list-style-type: none"> - HE with three-zonal type baffles - Turbulent flow - Optimization - Experimental study - Taguchi-method - Standard type k-ϵ - ANSYS Fluent 	

duct by inserting V-down baffles. The study concerned with the treatment of enhancing the heat transfer by using the roughness structure for the duct walls, where its various effects on the hydrothermal behavior were determined, and the largest heat transfer was obtained for a relative pitch ranging between 1.5 and 3. Using the technique of boundary elements as well as the approach of finite elements, Ghalandari et al. (2019) conducted numerical studies to examine various sloshing terms as well as the flexibility terms of elastic-type structures, submerged in a flow field. According to the obtained data, the change in the dimensions of the elastic structures, such as width, thicknesses as well as height, strongly changes the hydrodynamic behavior of the coupled system. Salih et al. (2019) conducted a detailed examination and full evaluation of the interactions between the moving limits of the thin-type structures and the flow fields by using numerical algorithms and methods. Akbarian et al. (2018) used natural-type gas for dual-fuel model engines through computational and applied studies. Additionally, Jedsadaratanachai and Boonloi (2014) and Sriromreun et al. (2012) determined flow friction along with thermal characteristic of a channel with V-shaped and Z-shaped baffles, respectively. Other theoretical and experimental experiments, such as Pourramezan et al. (2020), Saravanakumar et al. (2020), Nakhchi et al. (2020), Saleh et al. (2019), Yu et al. (2020), Promvongse and Skullong (2019a, 2019b, 2020), Ekiciler (2020), Eiamsa-ard and Chuwat-anakul (2020), Liang et al. (2019), Zhang et al. (2019)

and Biçer et al. (2020), considered and studied new physical models and domains with novel vortex generators as addressed below in Table 1.

According to other ways, many other studies have resorted to exploiting new fluids as a substitute for conventional fluids, i.e. air and water, as reported by Dogonchi et al. (2019, 2020); Hoseinzadeh et al. (2019); Mehryan et al. (2019); Alsabery et al. (2019); Kumar et al. (2020); Chamkha and Al-Mudhaf (2005); Chamkha et al. (2016, 2017); Zaraki et al. (2015); Gorla and Chamkha (2011); and Mohebbi et al. (2017); Takhar et al. (2001) for different thermal systems.

Solar air duct heat exchangers are involved in many applications such as heating, cooling and drying. Therefore, it is important to update these thermal devices by giving them an effective engineering structure by inserting new vortex generators such as 'V'-shaped obstacles. The finning technology has been the subject of many previous studies where fins in their traditional form have been used strongly. Also, some authors have considered other modern models, such as helical obstacles. Sure, this type of vortex generators is important in terms of performance, but it is complex in structure and difficult to achieve.

On the other hand, other new high-performance configurations have been used, according to different forms, such as V, W, and Z, where they can easily be exploited experimentally. Therefore, it is important to activate such models in raising the performance of some solar ducts

for air-heat exchangers by conducting research studies using the CFD codes. Through this research, we present a numerical simulation of thermal-aerodynamic characteristics of a solar air duct with multiple V-shaped baffles. The thermal-aerodynamic characteristics are listed below:

- The aerodynamic characteristics are: streamlines (or stream-function), mean, axial and transverse velocities, dynamic pressure, as well as local and average friction coefficients (or pressure drop).
- The thermal characteristics are: isotherms, as well as local and average Nusselt numbers.
- The thermal-aerodynamic characteristic is the thermal enhancement factor (Performance: *TEF*).

In this study, we focus mainly on important geometric variables related to V-fins, namely the attack angle, the height as well as the separation length between them, along with the flow rate, in order to reach an optimal solution for better conditions.

Conception of a duct provided by vortex V-generators

Figure 1 is a cross-section diagram of a 2-D horizontal rectangular duct model from an air-heat exchanger with novel fin-type obstacles in the upstream V-geometry in order to change the main flow path, to create recycling areas, to ensure good mixing, and to raise the transport of the heat from the hot regions to working fluid.

The new heat exchanger model, reported in Figure 1, has been prepared on the basis of empirical and numerical data from Demartini et al. (2004). In their studies, the airfield was treated in the case of a pair of vertical simple obstacles having a height (H_b) of 8×10^{-2} m and a thickness (w) of 10^{-2} m with a pitch (D_s) of 142×10^{-3} m, inside a heat exchanger of 146×10^{-3} m in height (H_c) and 167×10^{-3} m in aeraulic diameter (D_h).

This contribution aims to update this heat exchanger by introducing a new model of staggered upstream V-shaped fins as an alternative to simple obstacles. This

study conducts two-dimensional simulations to evaluate the hydrothermal and dynamic structure of the multi-finned duct in the presence of different attack angle (α), varying from 40° to 80° with respect to the horizon, and multiple heights, from $H_b/2$ to $3H_b/2$, with variable separation lengths, from $D_s/2$ to $5D_s/4$. Moreover, compared to other models of the ducts, such as smooth ducts or those supported by obstacles, i.e. 90° simple, downstream-type V, upstream-type V, trapezoidal, triangular, S, W and Z vortex generators, they are also highlighted and discussed in order to show the effectiveness of the current model.

The aeraulic boundary condition is considered to be a consistent 1-D velocity (U_{in}) at the duct's intake as provided in the literature (Demartini et al., 2004; Endres & Möller, 2001; Nasiruddin & Siddiqui, 2007). The air temperature is 300 K at section $x = 0$ (Nasiruddin & Siddiqui, 2007). The solid limits of the exchanger, as well as the fin installation bases, are kept to have 375 K constant temperature (Nasiruddin & Siddiqui, 2007). The conditions of wall limits are considered to be non-slip, and atmospheric pressure is applied in the exchanger outlet (Demartini et al., 2004). Additionally, the succeeding presumptions are considered to develop the hydrothermal improvement: both the air-fluid and the aluminum metal used have fixed properties, the aeraulic fluid is considered Newtonian as well as incompressible, while the flow is steady-state turbulent ($Re = 6 \times 10^3 - 3 \times 10^4$). Also, the radiation heat transfer is neglected.

Mathematical formulation and numerical solution

Under the abovementioned presumptions, the hydrothermal model is controlled by (Nasiruddin & Siddiqui, 2007):

The continuity:

$$\nabla \cdot \vec{V} = 0 \quad (1)$$

The momentum:

$$\rho(\vec{V} \cdot \nabla \vec{V}) = -\nabla P + \mu_f \nabla^2 \vec{V} \quad (2)$$

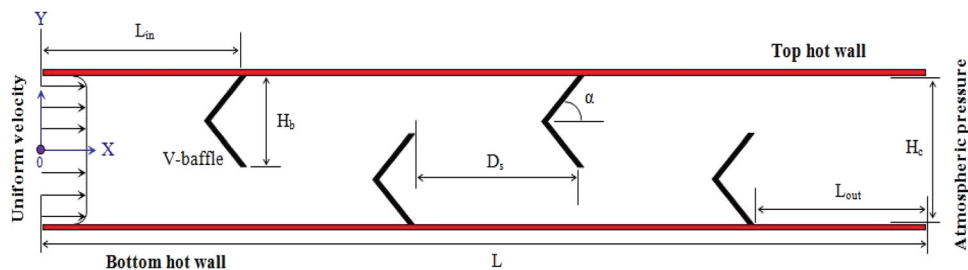


Figure 1. Staggered V-finned duct solar air-heat exchanger model.

The energy:

$$\rho C_p (\vec{V} \cdot \nabla T) = k_f \nabla^2 T \quad (3)$$

The turbulence phenomenon is mathematically modeled by using the k - ε model of standard-type (Launder & Spalding, 1974). It has a first equation, related to kinetic energy of turbulence (K), which is defined as below:

$$\frac{\partial}{\partial x_j} (\rho k u_j) = \frac{\partial}{\partial x_j} \left[\left(\mu + \frac{\mu_t}{\sigma_k} \right) \frac{\partial k}{\partial x_j} \right] + G_k + \rho \varepsilon \quad (4)$$

While the rate of dissipation of turbulence (ε) is the content of the second equation:

$$\frac{\partial}{\partial x_j} (\rho \varepsilon u_j) = \frac{\partial}{\partial x_j} \left[\left(\mu + \frac{\mu_t}{\sigma_\varepsilon} \right) \frac{\partial \varepsilon}{\partial x_j} \right] + C_{1\varepsilon} \frac{\varepsilon}{k} - C_{2\varepsilon} \rho \frac{\varepsilon^2}{k} \quad (5)$$

The aeraulic-diameter:

$$D_h = 2HW/(H + W) \quad (6)$$

The Reynolds-number:

$$Re = \rho \bar{U} D_h / \mu \quad (7)$$

The local-Nusselt-number:

$$Nu_x = \frac{h(x) D_h}{k_f} \quad (8)$$

The average-Nusselt-number:

$$Nu = \frac{1}{L} \int Nu_x \partial x \quad (9)$$

The Nusselt-number correlation of Dittus and Boelter (1930):

$$Nu_0 = 0.023 Re^{0.8} Pr^{0.4} \quad (10)$$

The local-friction-coefficient:

$$C_f = \frac{2\tau_w}{\rho \bar{U}^2} \quad (11)$$

The average-friction-coefficient:

$$f = \frac{2(\Delta P/L) D_h}{\rho \bar{U}^2} \quad (12)$$

The friction-factor correlation of Petukhov (1970)

$$f_0 = (0.79 \ln Re - 1.64)^{-2} \quad (13)$$

The performance-factor:

$$\eta = \frac{(Nu/Nu_0)}{(f/f_0)^{1/3}} \quad (14)$$

Furthermore in this study, the employed mesh structure is a 2-D, non-uniform grid. The refined mesh at all solid walls and limits is shown in Figure 2. This refinement is needed to have precise temperature gradients and velocity in the area under study. As illustrated in Figure 2, the mesh far from the walls is uniform.

This simulation has been tried out using two basic components, namely the computational technique of finite volumes (Patankar, 1980), Algorithm of discretization 'SIMPLE' (Patankar, 1980), through the software 'ANSYS Fluent 12.0 (2012)'. Additionally, Leonard and Mokhtari (1990)'s interpolation QUICK-scheme has been employed for the flow properties. And, for the pressure terms, a second-order upwind method (Patankar, 1980) was implemented, see Table 2.

On the other hand, the intensity of the mesh and its effect on the computational solution are investigated as shown in Table 3. The qualitative changes of maximum dynamic pressure (Pd_{max}) and x -velocity (u_{max}) values are analyzed by giving their relative percent errors, respectively, δ (see Eq. 15a) and δ' (see Eq. 15b), in the presence of different cell meshes.

$$\delta = \frac{Pd_{ref} - Pd}{Pd_{ref}} \times 100 \quad (15a)$$

$$\delta' = \frac{u_{ref} - u}{u_{ref}} \times 100 \quad (15b)$$

The least relative error is observed on the grid of 245×95 nodes, as it reached about 0.130% in the case

Table 2. Solution controls.

Discretization	
Pressure	Second-Order Upwind
Momentum	Quick
Kinetic energy of turbulence	Quick
Rate of dissipation of turbulence	Quick
Energy	Quick
Pressure-velocity coupling	SIMPLE

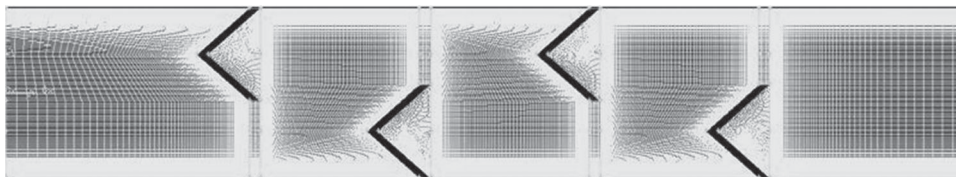


Figure 2. Used non-uniform grid.

Table 3. Mesh independence analysis ($\alpha = 60^\circ$, H_b , D_s , and $Re = 6 \times 10^3$).

N_x	95	120	145	170	195	220	245	370
N_y	35	45	55	65	75	85	95	145
Pd_{max}	2.875	2.912	2.946	3.007	3.019	3.052	3.063	3.067
δ	6.260	5.053	3.945	1.956	1.565	0.489	0.130	ref.
u_{max}	1.907	1.935	1.958	1.980	1.998	2.026	2.039	2.044
δ' (%)	6.702	5.332	4.207	3.131	2.250	0.880	0.244	ref.

of Pd_{max} while 0.244% in the case of u_{max} , by raising it to 370×145 cells. So, the grid of 245×95 cells is used for all simulations. Also for solution convergence, the normalized residuals are fixed at 10^{-9} for equations of continuity (Eq. 1), x - and y - velocities (Eq. 2); k (Eq. 4) and ε (Eq. 5), while 10^{-12} for the energy equation (Eq. 3).

In the beginning, an attempt is made to validate some predicted results against the experimental data of the literature. A reference is made to the experimental work realized by Demartini et al. (2004), which consists of a simple duct heat exchanger as that considered by Demartini et al. (2004). With the same geometrical conditions as those undertaken by these authors, the

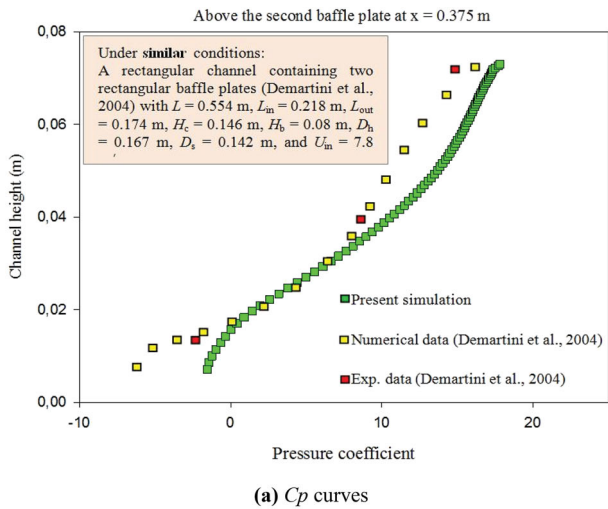
values of the pressure coefficient (C_p) above the second plate at $x = 0.375$ m are depicted in Figure 3a along with the exchanger height. Furthermore, the variation of axial velocity (u) in the upper part of the duct at $x = 0.525$ m (i.e. near the outlet section) is illustrated in Figure 3b. As clearly observed, the comparison of our numerical results with those obtained numerically and experimentally by Demartini et al. (2004) reveals a satisfactory agreement.

Another verification of the reliability of our numerical method is performed in Figure 4, where the effect of the turbulence models on some predicted results is inspected. Four turbulence models were examined for this purpose, namely: standard-type $k-\varepsilon$, RNG-type $k-\omega$, standard-type $k-\omega$, and SST-type $k-\omega$ models. The curves of axial velocity in the top region of the channel at $x = 0.525$ m and $U_{in} = 7.8$ m/s are presented in Figure 4 for the four studied models of the turbulence. These results are compared to the experimental data of Demartini et al. (2004). From this figure, it seems that the standard-type $k-\varepsilon$ is the model that gives the lowest deviation from the experimental data. Therefore, this model has been selected to achieve the next computations.

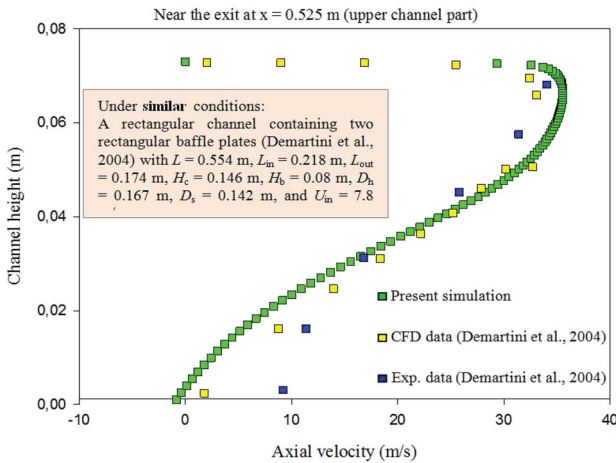
Results and discussion

Effect of the attack angle

In this section, the effect of attack angle of the V-fins (α) is examined. The α angle is changed from 40° to 90°



(a) C_p curves



(b) u curves

Figure 3. Validation curves.

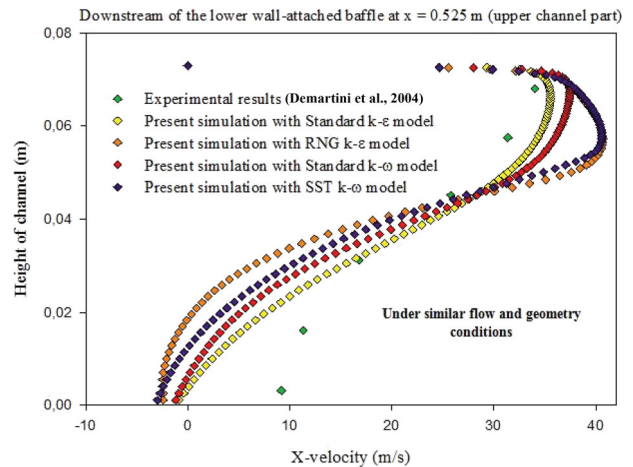


Figure 4. Effect of models of turbulence on the x -velocity curves, $U_{in} = 7.8$ m/s.

with a degree step of 10° , i.e. six geometrical cases were considered for constant V-fins' height and space values ($H_b = 0.08$ m and $D_s = 0.142$ m).

Figure 5a-g highlights the axial velocity field values for solar duct air-heat exchangers without or with vortex generators (VGs) according to different attack angles varying from 40 to 90 degrees, at $Re = 6 \times 10^3$. It is very clear that the current of air is stable in the absence of VGs. In the case of V-finned heat exchangers, the amounts of the x -velocity can be relatively negligible adjacent to the V-fins, specifically within the downstream zones since the recirculation areas exist. Away from these areas, the lines of the air-current turn into a parallel form that gradually engenders the flow development. It should be noticed that the x -velocity values increase in the area expanded from the VG end to the exchanger's wall. The reason for the x -velocity increase can be mentioned as using V-fins and creating the circulating motion in the duct. Thus, a sudden alter in the flow direction appears. Also, it can be noticed that the highest amount of x -velocity can be observed adjacent to the exchanger top for all V-fins. Furthermore, the V-fin's attach angle impacts the flow characteristics. If the attack angle (α) is increased, it leads to the flow deviation and acceleration adjacent to the V-fins which results in intensifying the convective rate of heat transfer. While this attack angle augmentation is restricted since it might cause the pressure drop to augment. It seems evident which more sensible effects on the upper left side of the V-fin can be seen by altering the V-angle (α) because of the air-field direction deviation. On the other hand, increasing the α angle from 80° to 90° increases the field intensity and enhances the recirculation cells, giving maximum values of x -velocity.

In terms of the velocity's transverse component (y -velocity), it is worth stating which for all the cases examined; negative y -velocity gradients can be noticed at the top-surface installed V-fin tip and positive y -velocity gradients at the bottom-surface placed V-fin end, Figure 6a-g. The y -velocity intensifies by enhancing α angle and consequently, the 90° case (simple baffle) provides maximum y -velocity.

Figure 7a-g illustrates the dynamic pressure (Pd) field distribution for airflow through the exchanger in the case of without or with VGs. As observed in this figure, the variation of the dynamic pressure is proportional to that of the attack angle (α). The data reported from simple baffle (of $\alpha = 90^\circ$) is also shown for comparison. Similarly to the x -velocity data in Figure 5 (a)–(e), the highest Pd values are presented in the vicinity of the duct's top wall, with an acceleration process which launches just following the fourth V-fin, as a consequence of the strong modifications in the flow direction in that region. The

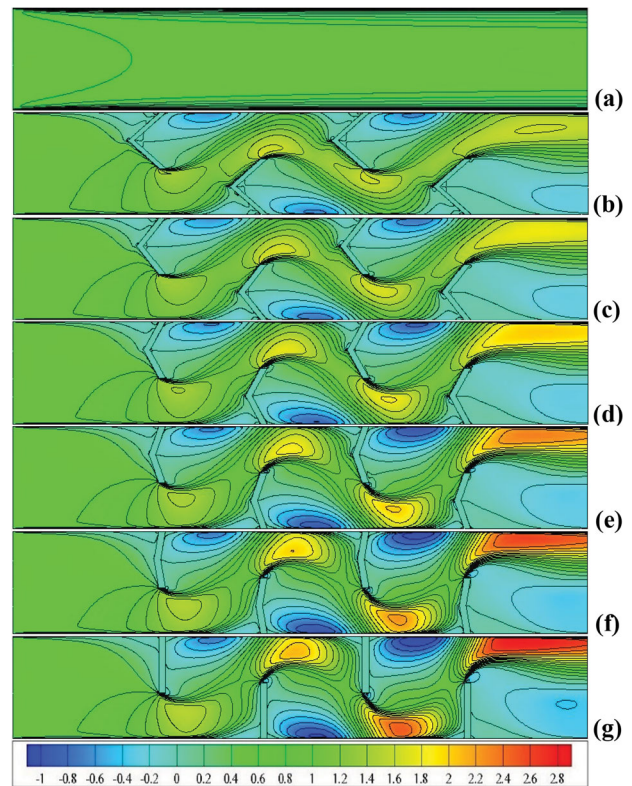


Figure 5. Fields of x -velocity for (a) smooth, and (b) 40° , (c) 50° , (d) 60° , (e) 70° , (f) 80° and (g) 90° finned heat exchangers with $Re = 6 \times 10^3$.

maximum dynamic pressure is obtained for $\alpha = 90^\circ$, while the lowest one is that for the cases with no VGs.

Figure 8a-g presents the distribution of the total temperature along with the exchanger for various cases, without or with different attack fins, namely $\alpha = 40^\circ, 50^\circ, 60^\circ, 70^\circ, 80^\circ$, and 90° . As shown in the 1st case, there is no evolution in temperature gradients for both hot surfaces due to the absence of VGs. Based on the other cases; it is obvious that the temperature alters considerably through the exchanger's hot wall for all VG cases. It can be concluded which the recirculation flows significantly affect the temperature field since superior fluid mixing can be achieved in the zones, between the heated sections and the center air areas. It leads to a great temperature gradient across the hot surface. Additionally, V-shaped baffles' attack angle spacing (α) influences the thermal field. Based on the above figure, it should be mentioned that temperature decreases significantly at $Re = 6 \times 10^3$ and for large α values. Thus, it can be concluded that the increase of the attack angle yields a decrease in the temperature of the air inside the exchanger.

Figure 9 proposes an analysis of the axial curves of velocity in the last section of the V-finned solar heat exchanger in order to assess the extent of their influence with the attack angle (α) and flow rates (Re).

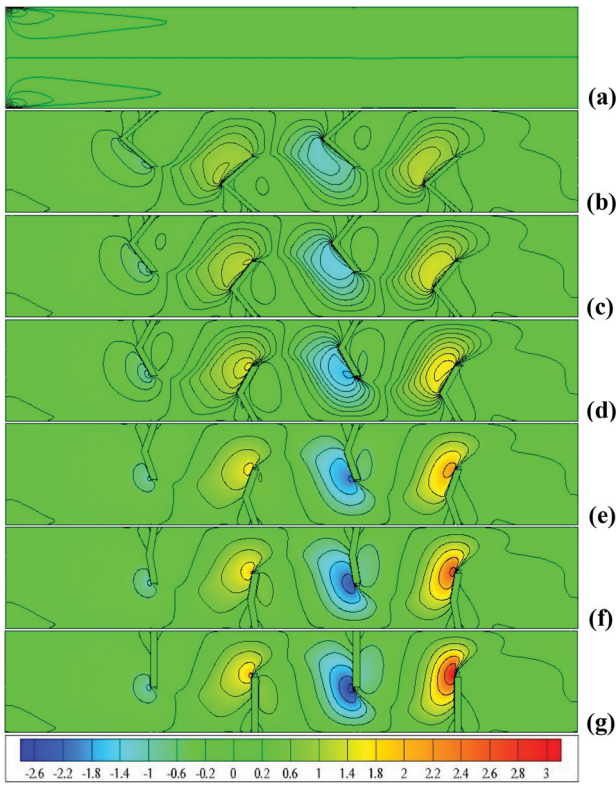


Figure 6. Fields of y -velocity for (a) smooth, and (b) 40°, (c) 50°, (d) 60°, (e) 70°, (f) 80° and (g) 90° finned heat exchangers with $Re = 6 \times 10^3$.

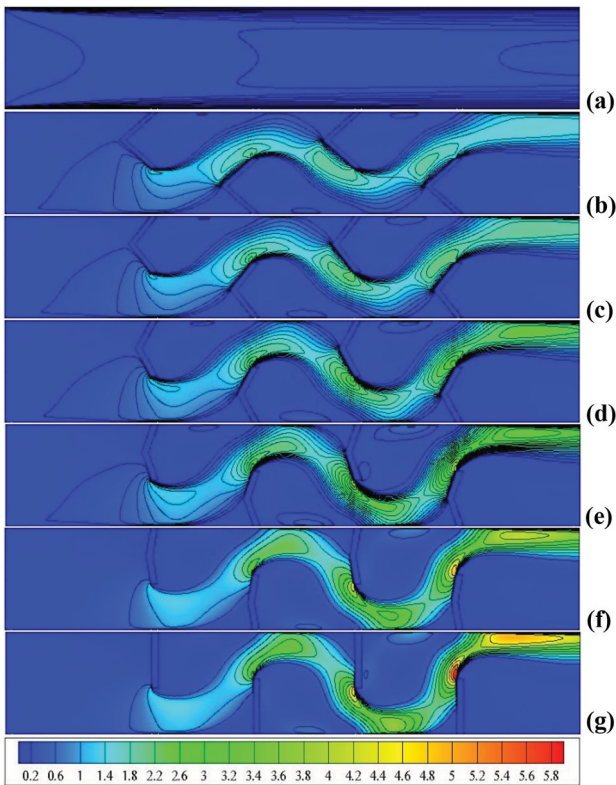


Figure 7. Fields of Pd for (a) smooth, and (b) 40°, (c) 50°, (d) 60°, (e) 70°, (f) 80° and (g) 90° finned heat exchangers with $Re = 6 \times 10^3$.

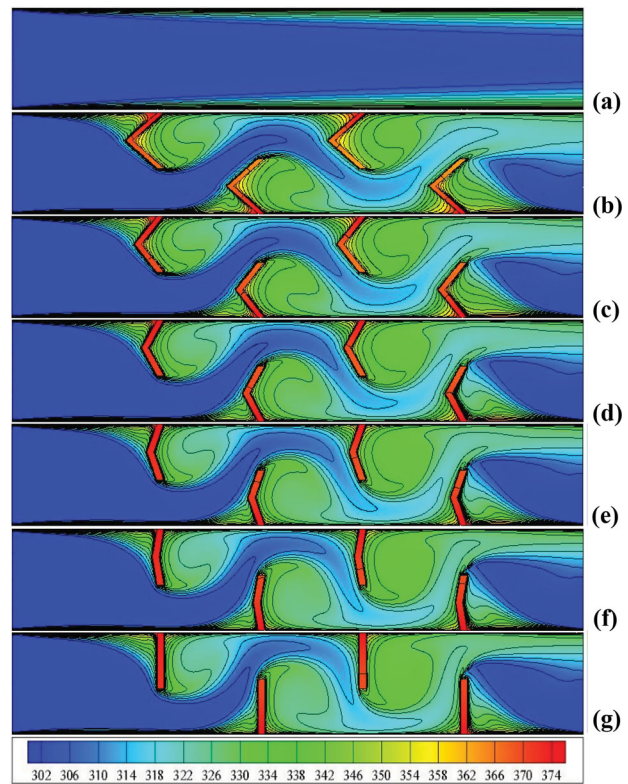
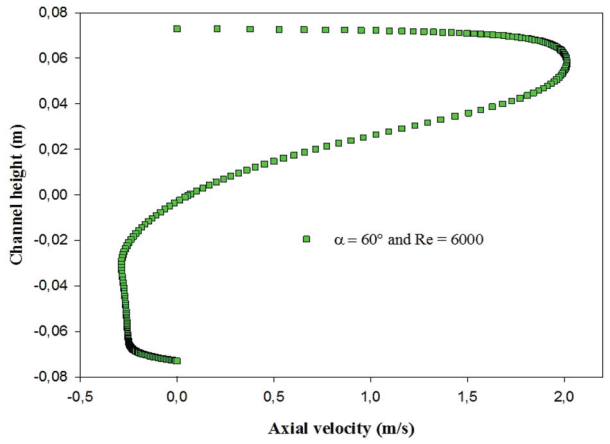


Figure 8. Fields of T for (a) smooth, and (b) 40°, (c) 50°, (d) 60°, (e) 70°, (f) 80° and (g) 90° finned heat exchangers with $Re = 6 \times 10^3$.

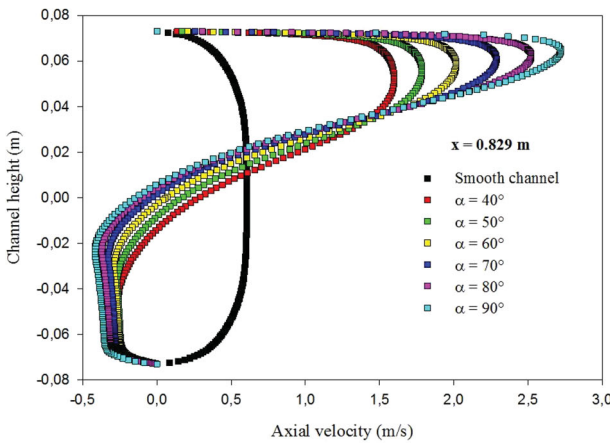
Next to the outlet of the exchanger, at an axial station equaled 0.829 m from the duct intake, 145 mm after the 4th VG as well as 29×10^{-3} m from the side right, and based on the outcomes in Figure 9a, the amount of velocity becomes around 2.00 m/s, that is 3.810 times higher than the U_{in} . It should be mentioned that extremely large recirculation to the back of the fourth fin led to these velocity values. The axial velocity is also presented plotted in Figure 9 versus the V-fins' attack angle, for a constant value of Re (of 6,000).

The curves indicate that the x -velocity improvement augments with increasing the attack value of α ; see Figure 9b. The smooth duct state is also under evaluation in this figure, which was characterized by low-value flat curves, as they were not subject to the effect of fins. The results given in Figure 9c indicate an increase of the axial velocity with the Re improvement.

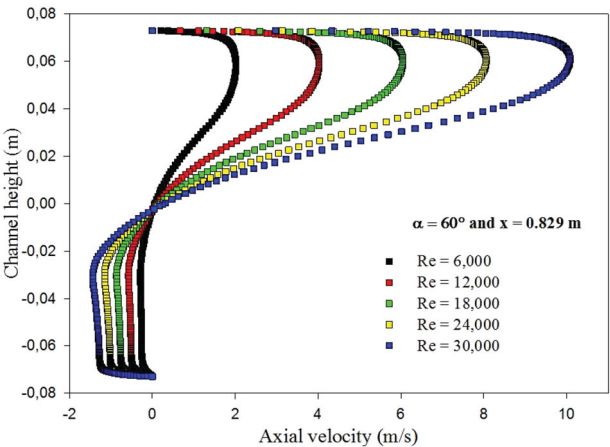
Figure 10 highlights the progression of the dimensionless local Nusselt number (Nu_x/Nu_0) measured across both lower ($y = -H/2$) and upper ($y = H/2$) exchanger walls at $\alpha = 60^\circ$ and $Re = 6 \times 10^3$. Based on the figure, the minimum value of Nu_x can be situated in the lowest part of the V-fins whereas the maximum amount can be achieved on its upper sections. In the intermediate zone, considerable values can be detected because of the fluid circulation between the V-fins. The achieved results are



(a) $\alpha = 60^\circ$ and $Re = 6 \times 10^3$



(b) $Re = 6 \times 10^3$ without or with different attack fins



(c) $\alpha = 60^\circ$ and $6 \times 10^3 \leq Re \leq 3 \times 10^4$

Figure 9. X-speed curves at $x = 0.829$ m for various situations.

in perfect conformity with all researchers who declare the appearance of the local recirculation areas. And this is associated with a higher heat transfer (as an illustration, see Nasiruddin & Siddiqui, 2007). Moreover, the dimensionless numbers of Nusselt are all greater than 1, about 50 times greater than that of the exchanger with no VGs,

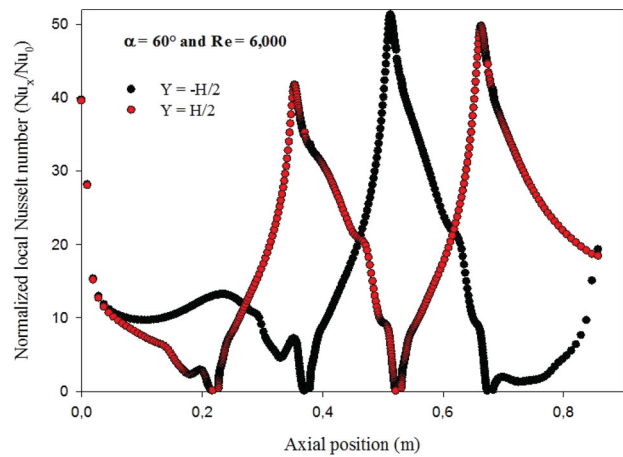
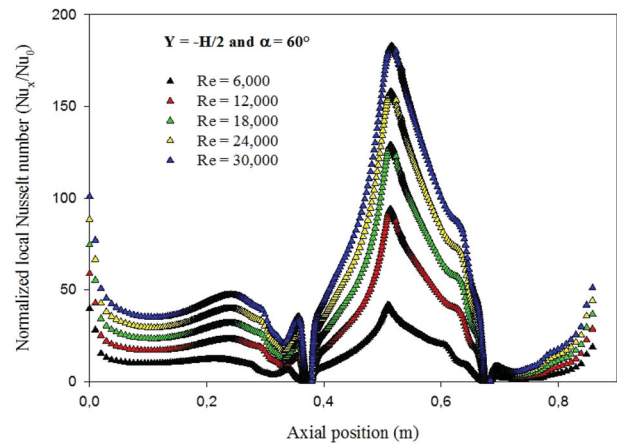
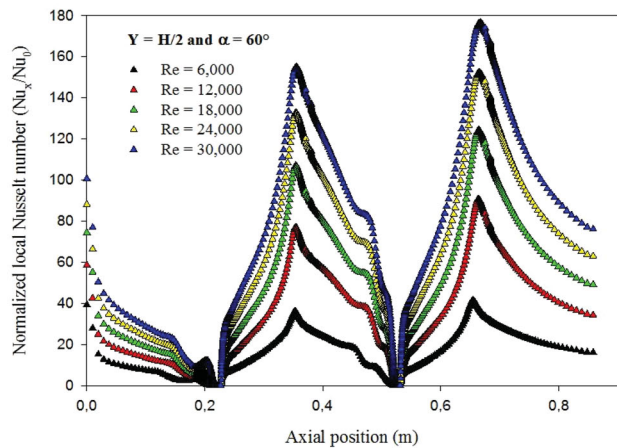


Figure 10. Nu_x/Nu_0 over the hot walls of the V-finned heat exchanger, $\alpha = 60^\circ$, $Re = 6 \times 10^3$.



(a) Lower wall ($y = -H/2$)



(b) upper wall ($y = H/2$)

Figure 11. Effect of rate of air on Nu_x/Nu_0 over the heat exchanger walls, $\alpha = 60^\circ$.

and this reflects the effectiveness of the fins present in the duct. Additionally, the rate of air affects the heat transfer. A linear increase can be detected between Re and Nu_x

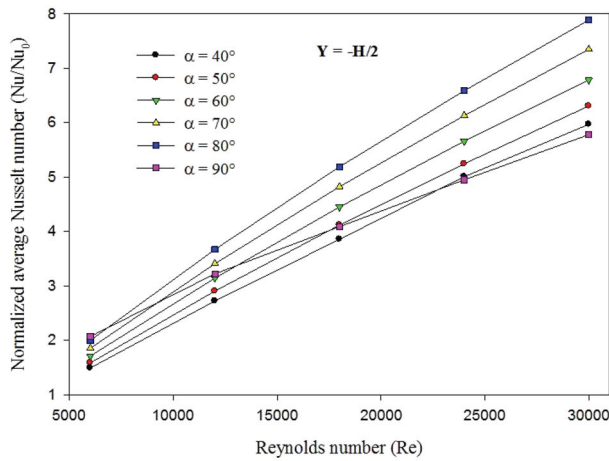
on both exchanger walls as listed in Figure 11a and b, respectively.

Figure 12 (a and b) reports the evolution of the dimensionless mean number of Nusselt (Nu/Nu_0) with air rate for various V-fin attack angles over the exchanger walls, $y = -H/2$ and $y = H/2$, respectively. It seems evident which the Nu/Nu_0 is considerably increased by augmenting the rate of air since the current speed increases in the two negative and positive ways. It is also worth stating which significant enhancements can be noticed for high, low, and medium flows. The outcome can be achieved since an enhancement in the rate of the fluid increases the circulation velocity together with the convective rate of transfer of heat from the exchanger wall. Consequently, the values of the Nu augment as well. Upper V- α value leads to an augmentation in the Nu values. The installation of 80° V-geometry VG performs much better than that of other 40° – 70° V-fins for increased Nu number. The maximum value of Nu is around 5.969, 6.307, 6.785,

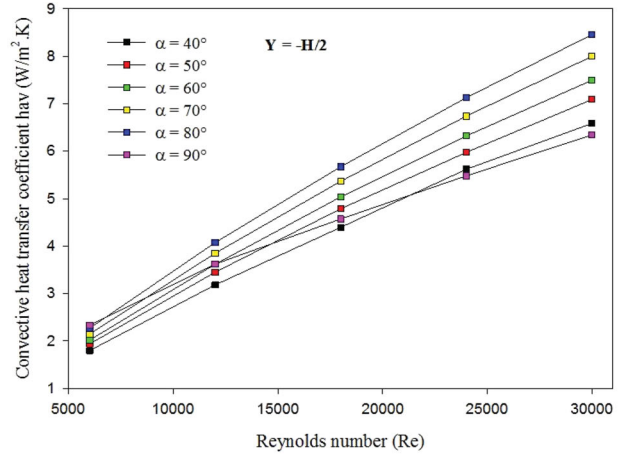
7.348 and 7.889 times larger than the smooth-walled exchanger, for $\alpha = 40^\circ, 50^\circ, 60^\circ, 70^\circ,$ and 80° , respectively, for $y = -H/2$ (see Figure 12a), while around 8.419, 8.900, 9.564, 10.314 and 11.015 times for $y = H/2$ (see Figure 12b).

However, the introduction of simple fins (of 90°) gives lower Nu values than that with $\alpha = 40^\circ, 50^\circ, 60^\circ, 70^\circ$ and 80° around 3.280, 9.113, 17.386, 27.130 and 36.484%, respectively, for $y = -H/2$ (see Figure 12a), while around 31.959, 39.493, 49.900, 61.667 and 72.648% for $y = H/2$ (see Figure 12b), at $Re = 3 \times 10^4$.

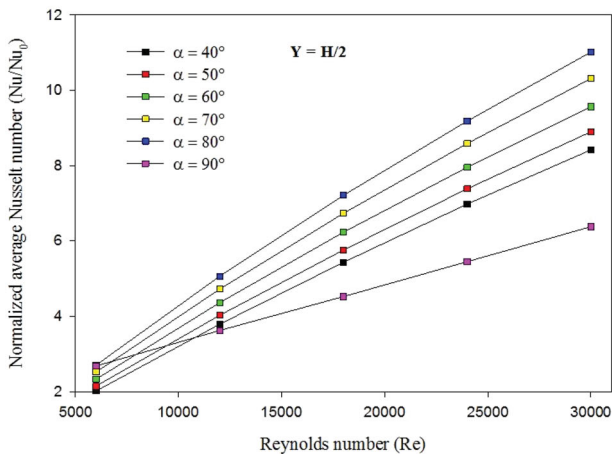
Figure 13 (a and b) presents the mean variations of the convective coefficient of transfer of heat (h_{av}) with the air rate at different attacks (α) over the exchanger walls, top and lower exchange surface, respectively. As expected, the obtained h_{av} employing the V-geometry fin with $\alpha = 80^\circ$ is substantially upper than that with smaller α values. At $Re = 3 \times 10^4$ and $y = -H/2$, the case of $\alpha = 80^\circ$ provides a value of h_{av} that is higher by about 22.142, 16.197,



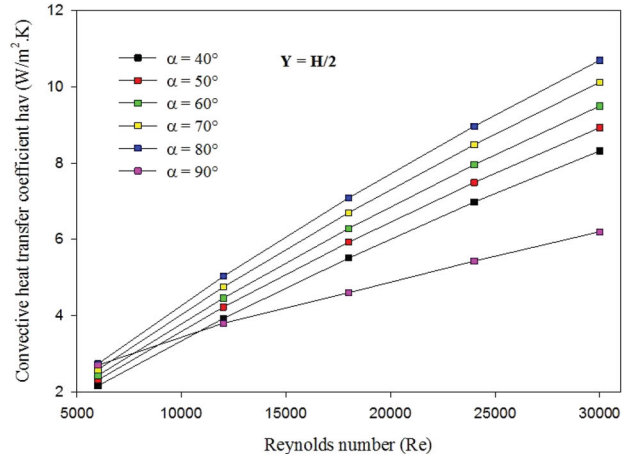
(a) Lower wall ($y = -H/2$)



(a) Lower wall ($y = -H/2$)



(b) upper wall ($y = H/2$)



(b) upper wall ($y = H/2$)

Figure 12. Effect of rate of air on Nu_x/Nu_0 over the exchanger walls for different attack V-fins.

Figure 13. Effect of rate of air on h_{av} over the exchanger walls for different attack V-fins.

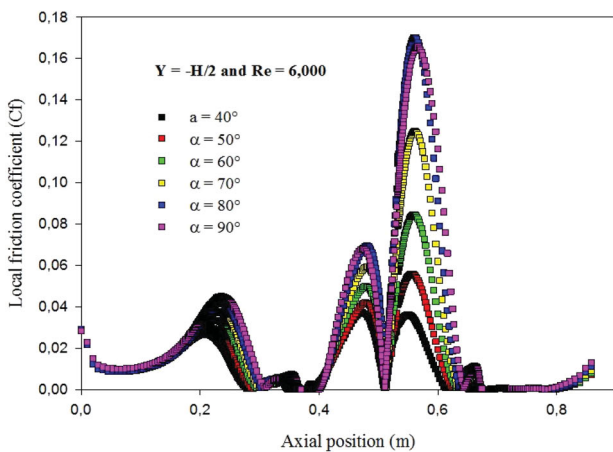
11.376 and 5.418% than those given with $\alpha = 40^\circ, 50^\circ, 60^\circ,$ and $70^\circ,$ respectively (see Figure 13a). However, and at $y = H/2,$ the superiority of the case $\alpha = 80^\circ$ in terms of h_{av} was about 22.221, 16.509, 11.219 and 5.356% over those reached by $\alpha = 40^\circ, 50^\circ, 60^\circ,$ and $70^\circ,$ respectively (see Figure 13b). It was also observed that the augmentation of Reynolds number yields an increase in h_{av} values for all α cases.

On the other hand, the presence of a simple fin, of 90° attack, reduces the h_{av} values by about 3.862, 11.794, 18.225, 26.173 and 33.401%; and 34.200, 44.056, 53.184, 63.301 and 72.543, compared to $\alpha = 40^\circ, 50^\circ, 60^\circ, 70^\circ$ and 80° cases, at $y = -H/2$ and $y = H/2,$ respectively.

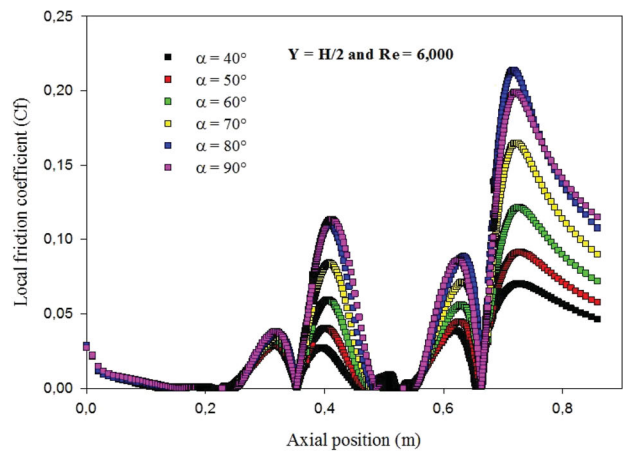
The regional variation of the coefficient of friction, C_f over $y = -H/2$ for V-geometry fins' attack angle values of $40^\circ \leq \alpha \leq 80^\circ$ and $Re = 6,000$ is illustrated below in Figure 14a. The smallest C_f is found around the lower surface-installed V-VGs, while the largest value is

encountered near the area confronting the upper wall-fixed V-fins. Moreover, the value of C_f augments for augmenting the V-angles. The effect of a simple VG on the C_f curves is also evident in Figure 14a, as it shows an increase in the values of friction across the lower gaps, due to the presence of the upper fins, with average values generated by the recycling cells. The skin friction coefficient is also influenced by the rate of air. It is clear that the C_f becomes more substantial once the Reynolds number augments; see Figure 14b.

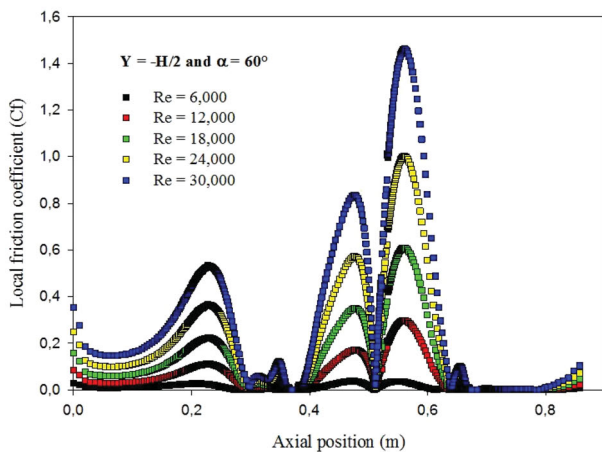
The axial change of C_f curves for the duct's hot top axis with distinct flow attack values at $Re = 6,000$ is graphed in Figure 15a. It seems obvious that the greatest amounts are initially adjacent to the duct's outlet since the fourth V-fin directs the flow towards the exchanger's upper part with great velocities and then in the intermediate zones since the fluid downstream of the upper wall-placed V-VG recirculates. Furthermore, the attack angle of the



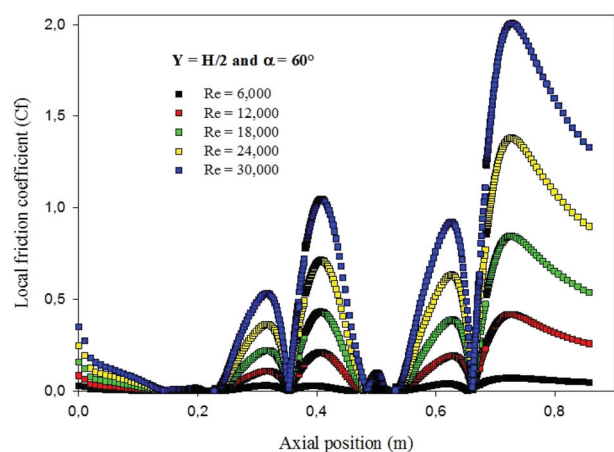
(a) Effect of α for $Re = 6,000$



(a) Effect of α for $Re = 6,000$



(b) Effect of Re for $\alpha = 60^\circ$



(b) Effect of Re for $\alpha = 60^\circ$

Figure 14. C_f over the lower exchanger wall for various situations.

Figure 15. C_f over the upper exchanger wall for various situations.

V-fin also affects the C_f value. A direct relationship is noted between C_f and α . The lowest C_f value was found at $\alpha = 40^\circ$, at all locations. This value augments as α goes up. The friction curves caused by the behavior of simple fins are also included in Figure 15a according to the same Re number used. A qualitative behavior similar to that reported by V-fins is recorded. Also, Figure 15b illustrates the impact of the flow rate on the axial progress of the skin friction coefficient C_f , with respect to Reynolds numbers. Identical results can be observed by this figure indicating C_f value is augmented by increasing the rate of air.

The curves are shown in Figure 16 stand out the progress of the average coefficient of friction, f with respect to the Reynolds number (6,000–30,000), at five various V-baffles' attack angle values ($\alpha = 40^\circ, 50^\circ, 60^\circ, 70^\circ,$ and 80°). Generally, the f has a tendency to augment with increasing Re . It can be noted that the improvement of the f factor is more significant than that of the Nu and h_{av} parameters. This might recommend which the turbulence fields and velocity enlarge faster than the isotherms. Based on the graph, it can be observed that the f factor augments once the V-geometry obstacles' attack angle (α) increases, independently from the Reynolds

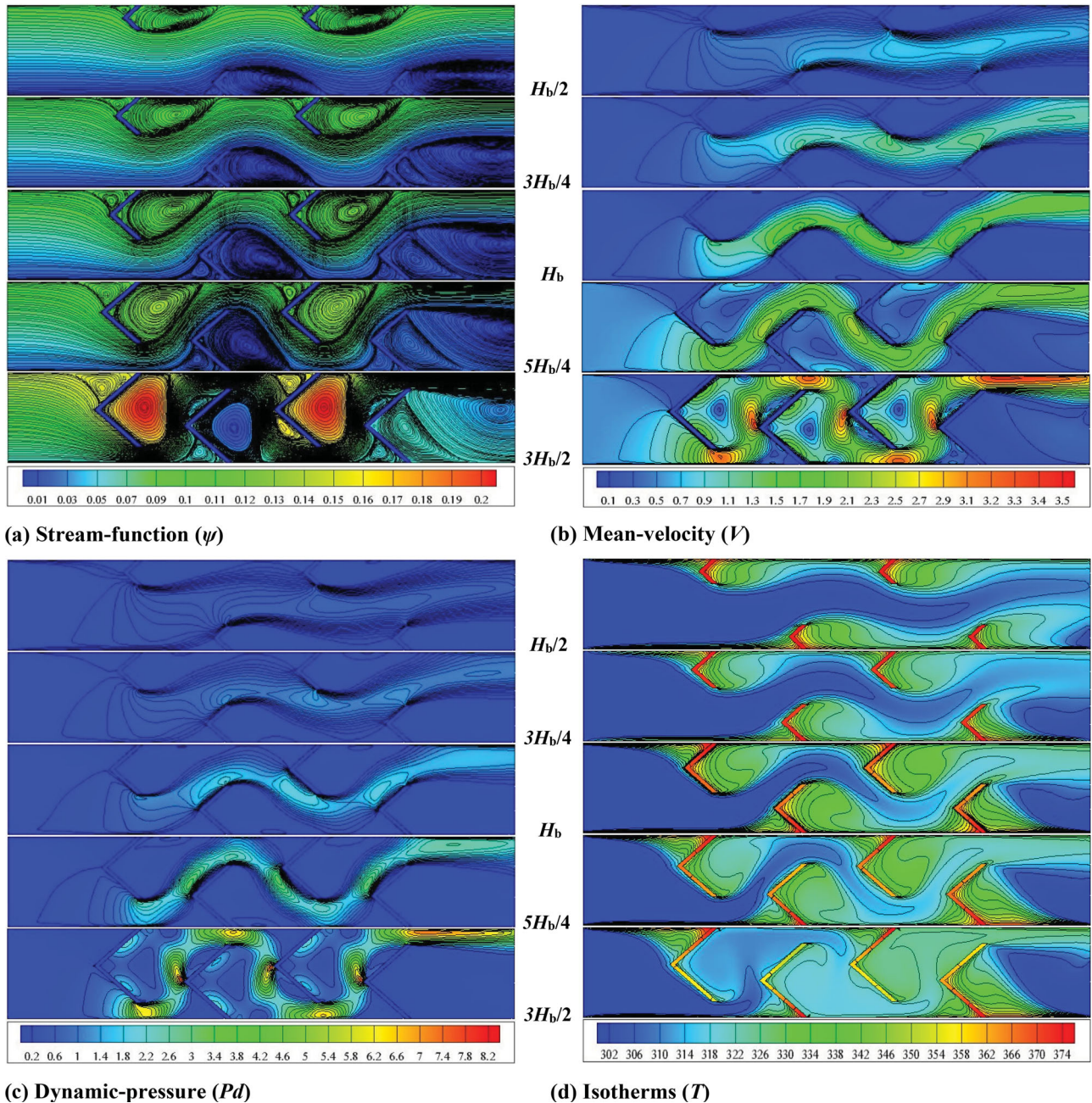
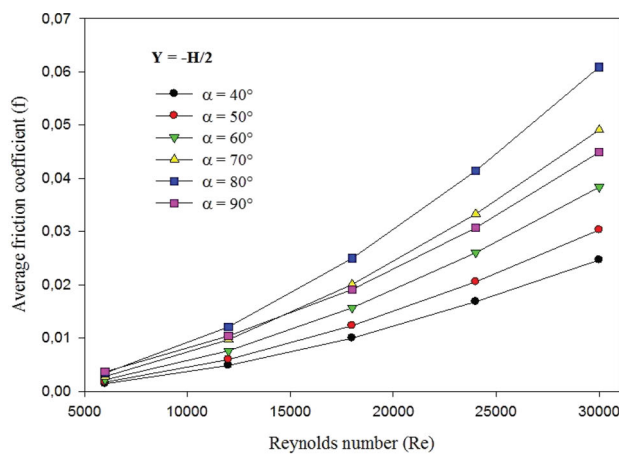


Figure 19. Hydrothermal fields for various 40°V-fins' heights, $D_s = 0.412$ m and $Re = 6,000$.

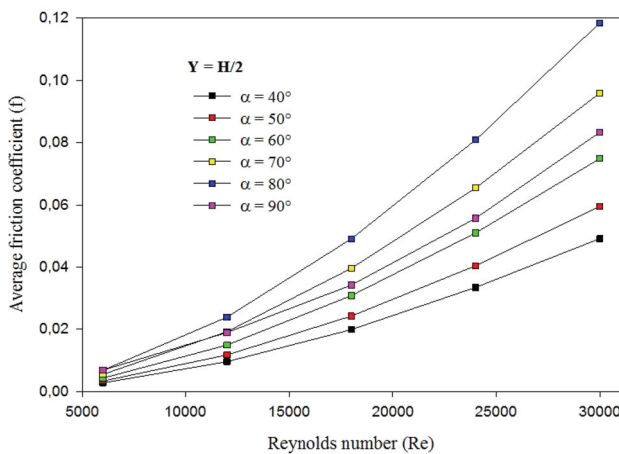
number. For an air rate of $Re = 3 \times 10^4$ and compared with the simple finned duct, of 90° , the insertion of V-fins with $\alpha = 70^\circ$, and 80° provided an elevation in the f factor, by about 9.354 and 35.634 percent, respectively, at $y = -H/2$ (see Figure 16a). However, at $y = H/2$ and for the same attack angles, the augmentation of the f factor was about 15.246 and 42.256 percent over the 90° finned duct (see Figure 16b). On the other hand, and at the same upper air rate, of 30,000, the superiority of the case $\alpha = 90^\circ$ in terms of friction was about 44.988%, 32.516% and 14.476%; and 41.056%, 28.571% and 10.084% over those reached by $\alpha = 40^\circ, 50^\circ, 60^\circ$, and 70° , at $y = -H/2$ and $y = H/2$, respectively.

Figure 17 assesses the performance (TEF) of all proposed finned duct heat exchangers for different α attacks from a specific range of rate of air. The TEF exceeded the value 1 in all considered cases, i.e. there is a hydrothermal improvement compared to the duct with smooth walls. In the case of large flow rates, the TEF drop for

V-finned ducts with smaller attack angle is determined to be greater than that with a larger attack angle. The TEF decreases by the increment in V-shaped baffles' attack angle (α) and thus, the $\alpha = 40^\circ$ provides maximum TEF.

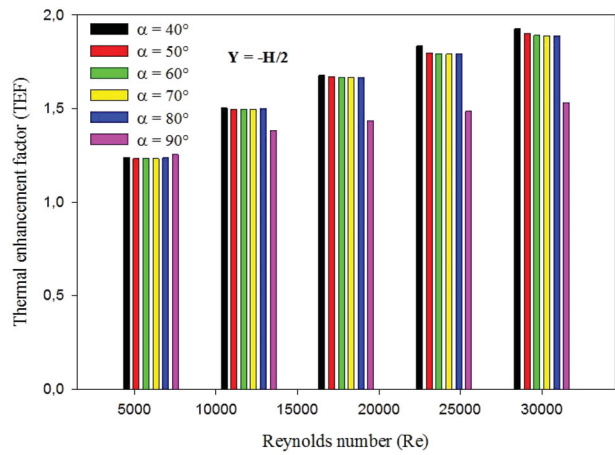


(a) lower wall ($y = -H/2$)

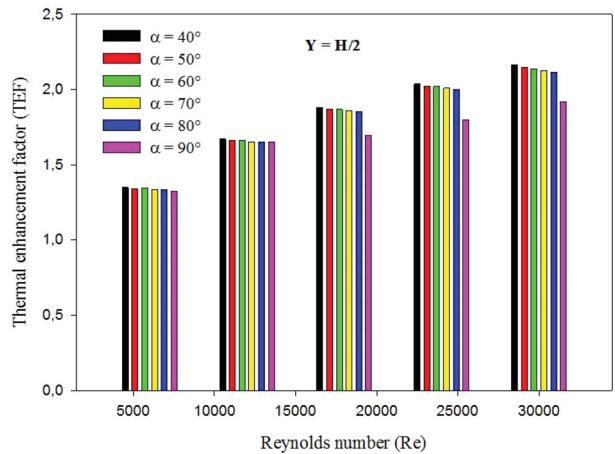


(b) upper wall ($y = H/2$)

Figure 16. Effect of rate of air on f over the exchanger walls for different attack V-fins.



(a) lower wall ($y = -H/2$)



(b) upper wall ($y = H/2$)

Figure 17. Performance evaluation for different V-finned heat exchangers.

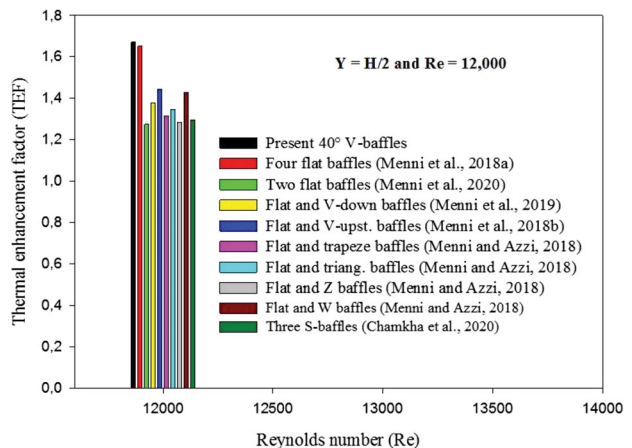


Figure 18. TEF comparison with other VG models.

The 50°, 60°, 70°, 80° and 90° attack fins present diminutions of about 1.323%, 1.775%, 1.936%, 1.957% and 20.577%, respectively, for $y = -H/2$ and $Re = 30,000$ (see Figure 17a), while about 0.744%, 1.159%, 1.770%, 2.158% and 11.267% for $y = H/2$ (see Figure 17b), in *TEF* relative to that in the 40° V-shaped fin indicating the 40° V-type baffle is more beneficial than the other cases.

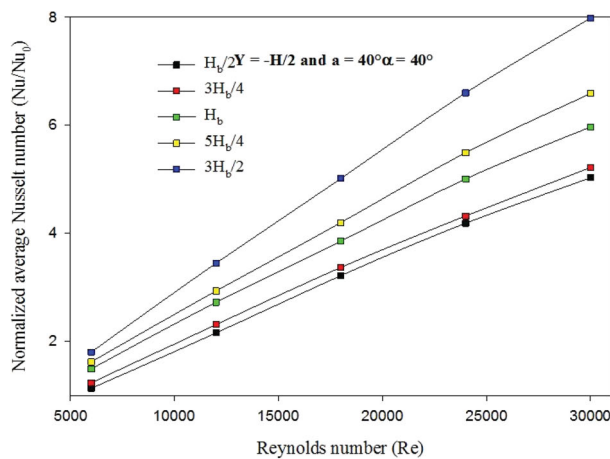
On the other hand, the current optimum V-fin of 40° was also evaluated along with other previous obstacle models from the literature as reported in Figure 18. For $Re = 1.2 \times 10^4$ and $y = H/2$, this fin exhibits an increase in *TEF* values of about 1.196%, 13.528%, 21.340%, 19.447%, 23.113%, 14.462%, 17.572%, 23.779% and 22.357% over that of cases with, four flat (Menni, Azzi, and Zidani, 2018); flat and upstream V (Menni, Azzi, Didi, et al., 2018), flat and trapezoidal (Menni & Azzi, 2018), flat and triangular (Menni & Azzi, 2018), flat and Z (Menni & Azzi, 2018), flat and W (Menni & Azzi,

2018), flat and down V (Menni et al., 2019), two rectangular (Menni et al., 2020), and three S- VGs (Chamkha et al., 2020), respectively.

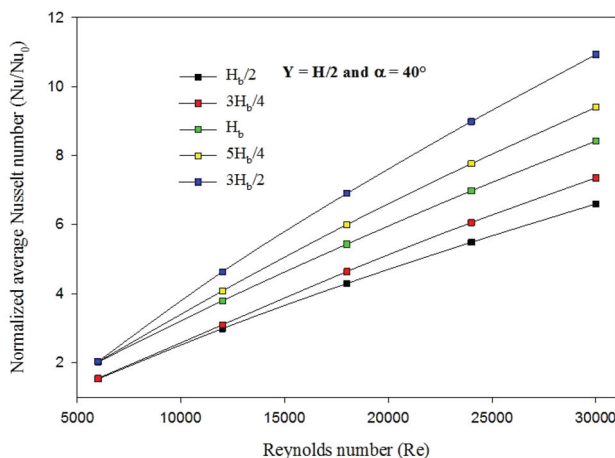
So, the current model according to the attack angle of 40° is considered as an ideal solution for determining the finned duct solar air-heat exchangers, especially in the case of high flow rates.

Effect of the 40° V-fin height

In this section, the effects of the V-fin height on the overall characteristics of the exchanger are highlighted for constant V-attack and space values ($\alpha = 40^\circ$ and $D_s = 0.142$ m). For this purpose, five geometrical configurations were realized, namely: 0.04, 0.06, 0.08, 0.10, and 0.12 m, respectively. These selected values of the V- height correspond to $H_b/2$, $3H_b/4$, H_b , $5H_b/4$, and $3H_b/2$, respectively.

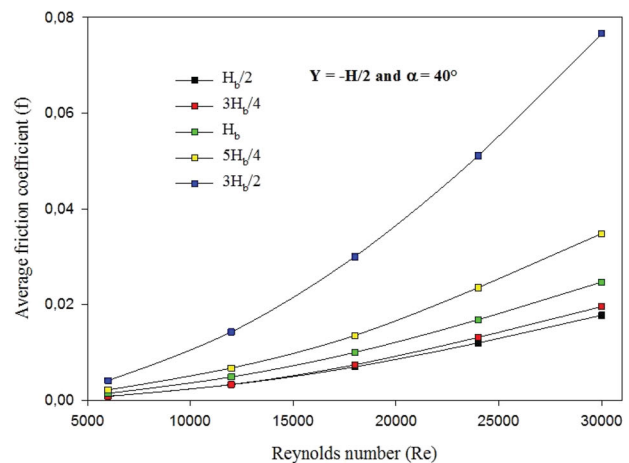


(a) lower wall ($y = -H/2$)

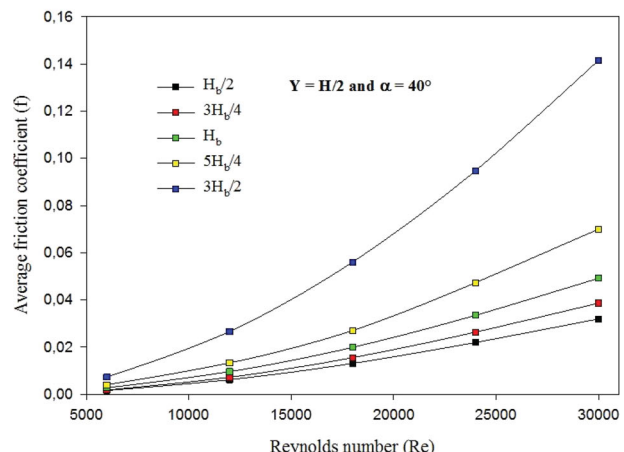


(b) upper wall ($y = H/2$)

Figure 20. Effect of rate of air on Nu/Nu_0 over the duct walls for different height 40°V-fins.



(a) lower wall ($y = -H/2$)



(b) upper wall ($y = H/2$)

Figure 21. Effect of rate of air on f over the exchanger walls for different height 40°V-fins.

The flow patterns induced for each geometrical case are illustrated in Figure 19a. It seems that the recirculation loops generated before and after the V-fin are enlarged with respect to the increasing value of V-length. The inclination of the segments of the V-fin by 40° presents a power generator of vortices, giving thus a strong interaction between the fluid particles. The mean velocity is also intensified with the rise, where the maximum value (V_{\max}) passed at $Re = 6,000$ from 1.106 to 3.577 m/s when the V-section height changed from 0.04 to 0.12 m, i.e. from $H_b/2$ to $3H_b/2$ (see Figure 19b). Furthermore, the excessive amount of V-height yields regions of strong velocities at the tip of each segment of the fin, with moderate or low velocities elsewhere.

These regions, where the high velocities occur, are also the location of significant values of the dynamic pressure (see Figure 19c). The maximum value of the pressure (Pd_{\max}) at $Re = 6,000$ passed from 0.749 Pa to 8.260 Pa when the V-length changed from 0.04 to 0.12 m, which corresponds to an increase by about 11 times compared with the case $H_b = 0.04$ m. This is mainly due to the flow behavior generated by this kind of vortex generators.

Certainly, the flow characteristics have a great impact on thermal behavior. From the plots provided in Figure 19d, the thermal fields are uniform until reaching the 1st V-fin, where the thermal exchange begins clearly. The heat exchange is then intensified gradually when the fluid passes through the next fins. Consequently, the increasing V-height reduces the required length in the exchanger to obtain the desired temperature of the fluid, which results in a compact exchanger.

Further details on the thermal exchanger are given in Figure 20a and b, where the values of the normalized Nu number, Nu/Nu_0 , are presented for the lower and upper hot walls of the duct, respectively. The variations of Nu/Nu_0 are presented for different values of Reynolds number and 40° V-fin height. The profiles of both figures confirm the finding illustrated in Figure 19d. The Nu/Nu_0 increases with the rise of the fin height. More precisely and for sizes, 0.04 and 0.12 m, respectively, the most significant values of Nu/Nu_0 are 5.028 and 7.983 on the lower wall of the duct, while 6.599 and 10.927 on the upper wall. These values are obtained at $Re = 3 \times 10^4$. Compared with the case $H_b = 0.04$ m, the normalized Nu number has been increased by about 1.587 and 1.655 times for the lower and upper walls of the duct, respectively.

In addition, the increase in Reynolds number produces an augmentation of the values of Nusselt number due to the intensification of the interaction between the fluid particles that is resulted in high Re . However, the friction factor is also increased on both walls of the exchanger with the rise of Re , as observed in Figure 21a and b. The

augmentation of the V-fin height has proved its efficiency in terms of enhancement of the thermal exchange, but the friction factor is also increased (see Figure 21). At $Re = 30,000$, the value of the friction factor passes from 0.017 to 0.076 on the lower wall, and from 0.031 to 0.141 on the upper wall, when H_b changed from $H_b/2$ to $3H_b/2$.

Finally, and aiming to give a global evaluation of the efficiency of the exchanger, the thermal enhancement factor (TEF) is determined for different flow rates and geometrical conditions (see Figure 22). For both walls of the duct, it seems that the TEF increases continually with the rise of the flow rates (Re). However, and when changing the V-fin height, the TEF increases until $H_b = 0.08$ m, then it decreases again. At $H_b = 0.08$, the values of TEF for the upper and lower walls of the exchanger are 2.163 and 1.926, respectively. The comparison between the values of the TEF on the lower and upper walls reveals a slight difference. It is slightly elevated in the case of $y = H/2$. This is maybe due to the strong gaps in the

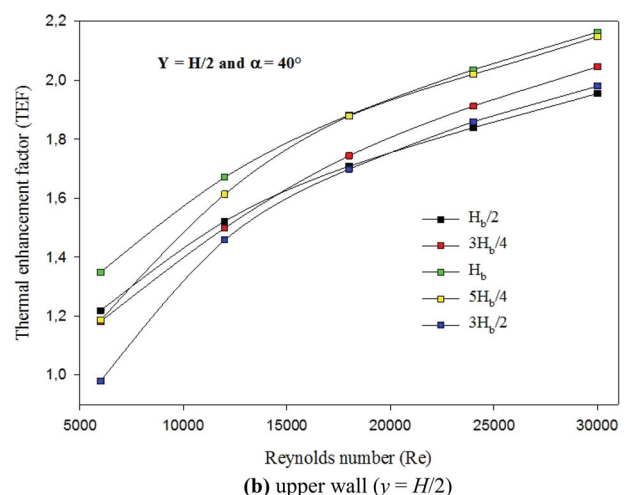
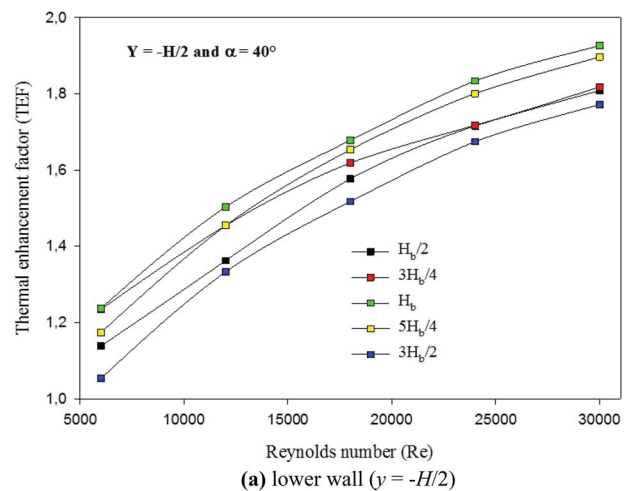


Figure 22. Performance evaluation for various height 40° V-fins.

upper exchanger side, in contact with the top horizontal axis, where they have high flow speeds, due to the high dynamic-pressure which produces high temperature gradients in the region and thus, an important heat transfer, in addition to the intensity of the recycling cells localized behind the upper V-fins.

Effect of the space between 40° V-fins

Another geometrical parameter that may affect the hydrothermal characteristics of the exchanger is studied in the section. It concerns the spacing between 40° V-fins (or the distance of separation). For this objective, four cases were considered, which are: 0.071, 0.1065, 0.142, and 0.1775 m. These values correspond to $D_s/2$, $3D_s/4$, D_s , and $5D_s/4$, respectively.

At $Re = 6,000$ and for an exchanger equipped with 40° V-fins having $H_b = 0.08$ m, the hydrodynamics induced

for the four cases are plotted in Figure 23a under a two-dimensional view. As observed, the location of the vortices is the same in each case. However, the intensity of these recirculation loops increases with the reduced distance of separation between the baffles. In the first case ($D_s/2$), the shape of the vortex developed after the first fin is highly affected by the second fin due to the small spacing between the VGs. The maximum value of the average velocity in this case ($D_s/2$) is the highest compared with the three other cases (see Figure 23b). It reaches 5.126 m/s at $D_s/2$, while it is only around 1.689 m/s at $5D_s/4$.

The dynamic-pressure is also strongly affected when changing the distance of separation between the fins (see Figure 23c). The most significant amount of the dynamic-pressure that is around 17.558 Pa is obtained with the 1st case ($D_s/2$), which is higher by about 10.038 times than the maximum value given by the last case ($5D_s/4$). This great difference in the Pd between the first and last cases

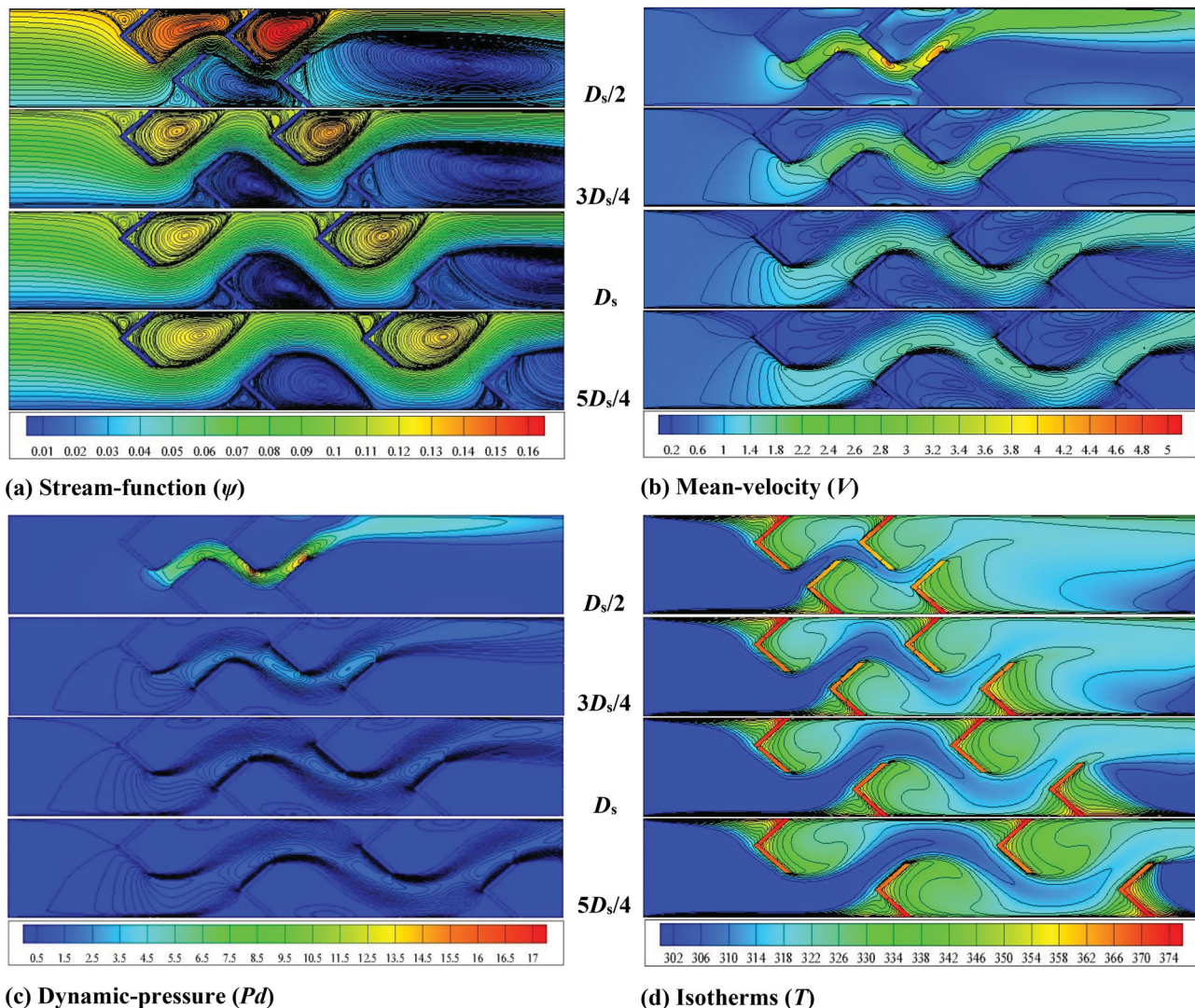


Figure 23. Hydrothermal fields for various 40°V-fins' spaces, $H_b = 0.08$ m and $Re = 6,000$.

is resulted by the wall effect, which increases furthermore with the reduced space between the VGs.

The intensification of the interaction between the fluid particles that is resulted by the small distance of separation promotes the heat transfer rates. As observed in Figure 23d, the cold fluid is rapidly heated during its passage through the finned region of the exchanger when the distance D_s is small. Therefore, the case $D_s/2$ may be selected as the most efficient in terms of enhanced thermal exchange. In addition, the increasing space between the vortex generators participates in the augmentation of the length in the duct that is required to obtain the desired temperature of the fluid.

Further insight into the convection phenomenon that is generated when changing the flow rate (Reynolds number), and the V-space (spacing) is provided in Figure 24a and b. In these figures, the normalized values of Nusselt number Nu/Nu_0 are given for the lower and upper walls of the exchanger, respectively. Increasing values of the Nu/Nu_0 are observed with the rise of Re . However,

an inverse proportionality is remarked when increasing the V-fins' distance. However, similar behavior of the variation of Nu/Nu_0 is shown for both walls of the exchanger. Overall, the most significant values of Nu/Nu_0 are reached at the highest Re ($= 30,000$ here) and $D_s/2$, which are 6.661 and 9.111 on the lower and upper walls, respectively. While the lowest values of Nu/Nu_0 at the same Re (30,000) are those of $5D_s/4$, which are 5.755 and 8.204 on the lower and upper walls, respectively.

The reduced distance between 40° V-fins has been found to be advantageous in terms of improvement of the heat transfer. However, the friction factor (f) has also been increased accordingly. The variation of f vs. D_s and Re is highlighted in Figure 25. At $Re = 30,000$, the highest amount of f is reached with $D_s/2$, and it is equal to 0.0379 and 0.0624 on the lower and upper walls, respectively. At the same Re , the lowest values of f are 0.0185 and 0.0430 on the lower and upper walls, respectively. The analysis of these results reveals an increase in the friction factor by about 204.864% and 145.116% on the lower and

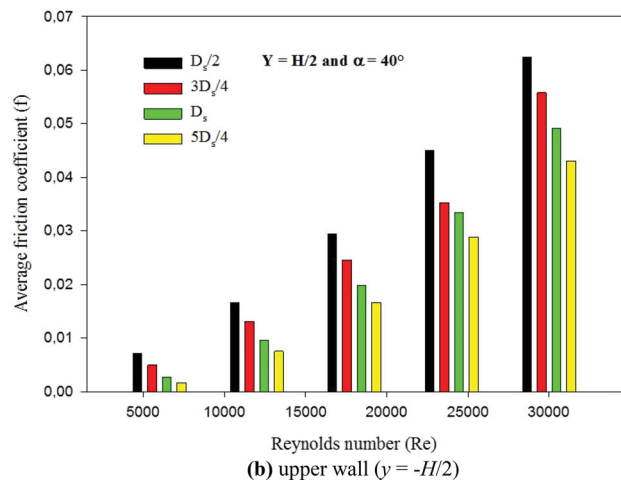
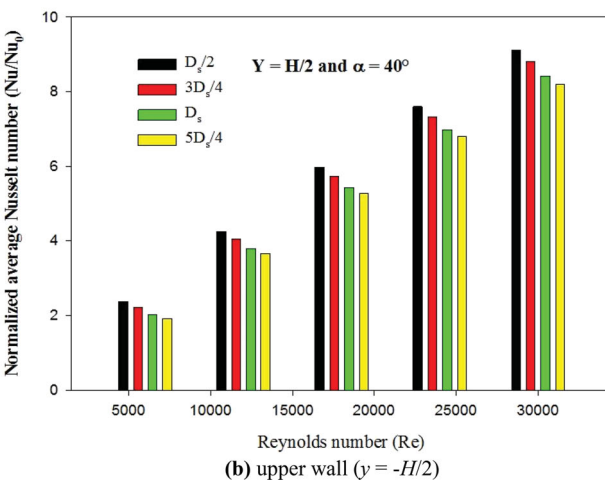
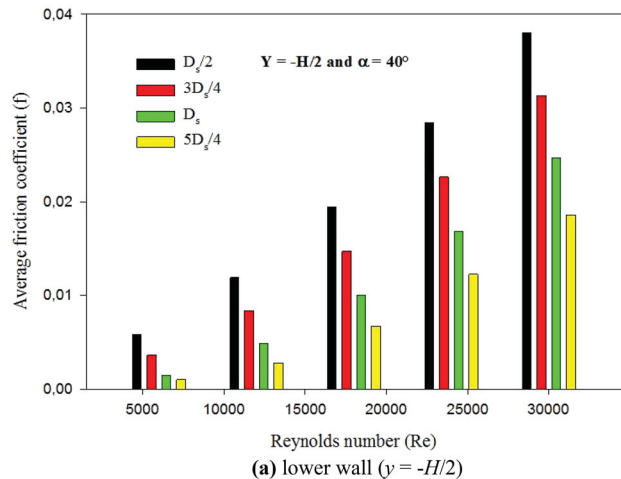
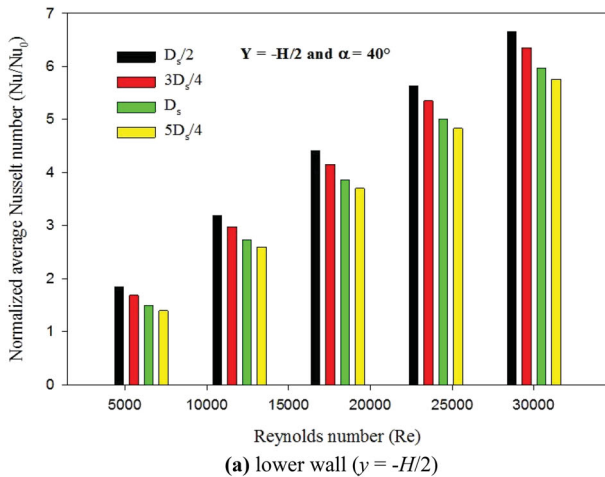


Figure 24. Effect of rate of air on Nu/Nu_0 over the duct walls for various 40° V-fins' spaces.

Figure 25. Effect of rate of air on f over the exchanger walls for various 40° V-fins' spaces.

upper walls, respectively, when the space between V-fin is changing from $5D_s/4$ to $D_s/2$.

Conclusions

In this research work, it is focused mainly on important geometric variables related to V-finned duct solar air-heat exchangers, namely the attack angle (40° – 90°), the height ($H_b/2$ – $3H_b/2$) as well as the separation length between VGs ($D_s/2$ – $5D_s/4$), along with the flow rate (6,000–30,000), to reach an optimal solution for hydrodynamic behavior and heat transfer performance.

The V-fin's attach angle impacts the flow and heat transfer characteristics. If the attack angle (α) is increased, it leads to the flow deviation and acceleration adjacent to the V-fins, which results in intensifying the convective rate of heat transfer. While this attack angle augmentation is restricted since it might cause the pressure loss to augment. It seems evident which more sensible effects on the upper left side of the V-fin can be seen by altering the V-angle (α) because of the air-field direction deviation. On the other hand, increasing the α angle from 80° to 90° increases the field intensity and enhances the recirculation cells, giving maximum values of x - and y -velocities. Additionally, V-shaped fins' attack angle spacing (α) influences the thermal field. Based on the considered attack values, it should be mentioned that temperature decreases significantly for large α values. Thus, it can be concluded that the increase of the attack angle yields a decrease in the temperature of the air inside the exchanger. The heat transfer in terms of Nu number is around 5.969, 6.307, 6.785, 7.348 and 7.889 times larger than the smooth-walled exchanger, for $\alpha = 40^\circ, 50^\circ, 60^\circ, 70^\circ,$ and 80° , respectively, for $y = -H/2$, while around 8.419, 8.900, 9.564, 10.314 and 11.015 times for $y = H/2$. However, the introduction of simple fins, of 90° , gives lower Nu values than that with $\alpha = 40^\circ, 50^\circ, 60^\circ, 70^\circ$ and 80° around 3.280, 9.113, 17.386, 27.130 and 36.484%, respectively, for $y = -H/2$, while around 31.959, 39.493, 49.900, 61.667 and 72.648% for $y = H/2$, at $Re = 3 \times 10^4$. Furthermore, the attack angle of the V-fin also affects the f value. A direct relationship is noted between f and α . The lowest f value was found at $\alpha = 40^\circ$, at all locations. For a maximum air rate and compared with the simple finned duct, of 90° , the insertion of V-fins with $\alpha = 70^\circ$, and 80° provided an elevation in the f factor, by about 9.354 and 35.634 percent, respectively, at $y = -H/2$. However, at $y = H/2$ and for the same attack angles, the augmentation of the f factor was about 15.246 and 42.256 percent over the 90° finned duct. On the other hand, and at the same upper air rate, of 30,000, the superiority of the case $\alpha = 90^\circ$ in terms of friction was about

44.988%, 32.516% and 14.476%; and 41.056%, 28.571% and 10.084% over those reached by $\alpha = 40^\circ, 50^\circ, 60^\circ,$ and 70° , at $y = -H/2$ and $y = H/2$, respectively. In terms of the performance, The TEF decreases by the increment in V-shaped baffles' attack angle (α) and thus, the $\alpha = 40^\circ$ provides maximum TEF . The $50^\circ, 60^\circ, 70^\circ, 80^\circ$ and 90° attack fins present diminutions of about 1.323%, 1.775%, 1.936%, 1.957% and 20.577%, respectively, for $y = -H/2$ and $Re = 30,000$, while about 0.744%, 1.159%, 1.770%, 2.158% and 11.267% for $y = H/2$, in TEF relative to that in the 40° V-shaped fin indicating the 40° V-type baffle is more beneficial than the other cases.

On the other hand, improving the length of the V-fins or decreasing in the space between them, increases the flow strength by enlarging the recycling cells, which reflects on the hydrodynamic behavior and changes the heat transfer. The presence of this new model of fins also highlights a hydrothermal improvement ranging between 1.196 and 23.779 percent compared to the previously mentioned models, reflecting the effectiveness of the new system of solar heat exchangers with air V-finned ducts. So, the current model according to the attack angle of 40° is considered as an ideal solution for determining the finned duct solar air-heat exchangers, especially in the case of high flow rates.

For future studies, the introduction of pores in the V-geometry baffles may provide further reduction in the pressure drop. The newly suggested design of VGs may also participate in the elimination of the low heat transfer areas (LHTA) that form behind the baffles. It is also proposed to examine the performance of the optimized geometrical configuration presented in our study (40° V-baffle) for other industrial applications, such as the cooling of complex non-Newtonian fluids.

Disclosure statement


No potential conflict of interest was reported by the author(s).

ORCID

Younes Menni  <http://orcid.org/0000-0003-1475-3743>

Mahyar Ghazvini  <http://orcid.org/0000-0002-3647-2101>

Houari Ameur  <http://orcid.org/0000-0003-2087-7574>

Mohammad Hossein Ahmadi  <http://orcid.org/0000-0002-0097-2534>

Mohsen Sharifpur  <http://orcid.org/0000-0003-1302-1954>

Milad Sadeghzadeh  <http://orcid.org/0000-0001-8574-5463>

References

- Abuşka, M. (2018). Energy and exergy analysis of solar air heater having new design absorber plate with conical surface. *Applied Thermal Engineering*, 131, 115–124. <https://doi.org/10.1016/j.applthermaleng.2017.11.129>

- Ahmadi, M. H., Baghban, A., Sadeghzadeh, M., Zamen, M., Mosavi, A., Shamshirband, S., Kumar, R., & Mohammadi-Khanaposhtani, M. (2020). Evaluation of electrical efficiency of photovoltaic thermal solar collector. *Engineering Applications of Computational Fluid Mechanics*, 14(1), 545–565. <https://doi.org/10.1080/19942060.2020.1734094>
- Akbadian, E., Najafi, B., Jafari, M., Ardabili, S. F., Shamshirband, S., & Chau, K. W. (2018). Experimental and computational fluid dynamics-based numerical simulation of using natural gas in a dual-fueled diesel engine. *Engineering Applications of Computational Fluid Mechanics*, 12(1), 517–534. <https://doi.org/10.1080/19942060.2018.1472670>
- Alsabery, A. I., Mohebbi, R., Chamkha, A. J., & Hashim, I. (2019). Effect of local thermal non-equilibrium model on natural convection in a nanofluid-filled wavy-walled porous cavity containing inner solid cylinder. *Chemical Engineering Science*, 201, 247–263. <https://doi.org/10.1016/j.ces.2019.03.006>
- Ameur, H. (2020). Effect of corrugated baffles on the flow and thermal fields in a channel heat exchanger. *Journal of Applied and Computational Mechanics*, 6(2), 209–218. <https://doi.org/10.22055/jacm.2019.28936.1521>
- Ameur, H., & Menni, Y. (2019). Laminar cooling of shear thinning fluids in horizontal and baffled tubes: Effect of perforation in baffles. *Thermal Science and Engineering Progress*, 14, 100430. <https://doi.org/10.1016/j.tsep.2019.100430>
- Amraoui, M. A., & Aliane, K. (2018). Three-dimensional analysis of air flow in a flat plate solar collector. *Periodica Polytechnica Mechanical Engineering*, 62(2), 126–135. <https://doi.org/10.3311/PPme.11255>
- ANSYS Fluent 12.0, Theory Guide, Ansys Inc., 2012.
- Beyaztas, U., Salih, S. Q., Chau, K. W., Al-Ansari, N., & Yaseen, Z. M. (2019). Construction of functional data analysis modeling strategy for global solar radiation prediction: Application of cross-station paradigm. *Engineering Applications of Computational Fluid Mechanics*, 13(1), 1165–1181. <https://doi.org/10.1080/19942060.2019.1676314>
- Bıçer, N., Engin, T., Yaşar, H., Büyükkaya, E., Aydın, A., & Topuz, A. (2020). Design optimization of a shell-and-tube heat exchanger with novel three-zonal baffle by using CFD and taguchi method. *International Journal of Thermal Sciences*, 155, 106417. <https://doi.org/10.1016/j.ijthermalsci.2020.106417>
- Boonloi, A., & Jedsadaratanachai, W. (2016). Numerical investigation on turbulent forced convection and heat transfer characteristic in a square channel with discrete combined V-baffle and V-orifice. *Case Studies in Thermal Engineering*, 8, 226–235. <https://doi.org/10.1016/j.csite.2016.07.003>
- Bopche, S. B., & Tandale, M. S. (2009). Experimental investigations on heat transfer and frictional characteristics of a turbulator roughened solar air heater duct. *International Journal of Heat and Mass Transfer*, 52(11-12), 2834–2848. <https://doi.org/10.1016/j.ijheatmasstransfer.2008.09.039>
- Cao, X., Du, T., Liu, Z., Zhai, H., & Duan, Z. (2019). Experimental and numerical investigation on heat transfer and fluid flow performance of sextant helical baffle heat exchangers. *International Journal of Heat and Mass Transfer*, 142, 118437. <https://doi.org/10.1016/j.ijheatmasstransfer.2019.118437>
- Chamkha, A. J., & Al-Mudhaf, A. (2005). Unsteady heat and mass transfer from a rotating vertical cone with a magnetic field and heat generation or absorption effects. *International Journal of Thermal Sciences*, 44(3), 267–276. <https://doi.org/10.1016/j.ijthermalsci.2004.06.005>
- Chamkha, A. J., Doostanidezfuli, A., Izadpanahi, E., & Ghalambaz, M. (2017). Phase-change heat transfer of single/hybrid nanoparticles-enhanced phase-change materials over a heated horizontal cylinder confined in a square cavity. *Advanced Powder Technology*, 28(2), 385–397. <https://doi.org/10.1016/j.apt.2016.10.009>
- Chamkha, A., Ismael, M., Kasaeipoor, A., & Armaghani, T. (2016). Entropy generation and natural convection of CuO-water nanofluid in C-shaped cavity under magnetic field. *Entropy*, 18(2), 50. <https://doi.org/10.3390/e18020050>
- Chamkha, A. J., Menni, Y., & Ameur, A. (2020). Thermal-aerodynamic performance measurement of air heat transfer fluid mechanics over S-shaped fins in shell-and-tube heat exchangers. *Journal of Applied and Computational Mechanics*. <https://doi.org/10.22055/JACM.2020.32107.1970>
- Chamoli, S., & Thakur, N. S. (2016). Correlations for solar air heater duct with V-shaped perforated baffles as roughness elements on absorber plate. *International Journal of Sustainable Energy*, 35(1), 1–20. <https://doi.org/10.1080/14786451.2013.857318>
- Demartini, L. C., Vielmo, H. A., & Möller, S. V. (2004). Numeric and experimental analysis of the turbulent flow through a channel with baffle plates. *Journal of the Brazilian Society of Mechanical Sciences and Engineering*, 26(2), 153–159. <https://doi.org/10.1590/S1678-58782004000200006>
- Dittus, F. W., & Boelter, L. M. K. (1930). Heat transfer in automobile radiators of tubular type. *International Communications in Heat and Mass Transfer*, 12(1), 3–22. <https://doi.org/10.1016/0735-1933>
- Dogonchi, A. S., Armaghani, T., Chamkha, A. J., & Ganji, D. D. (2019). Natural convection analysis in a cavity with an inclined elliptical heater subject to shape factor of nanoparticles and magnetic field. *Arabian Journal for Science and Engineering*, 44(9), 7919–7931. <https://doi.org/10.1007/s13369-019-03956-x>
- Dogonchi, A. S., Tayebi, T., Chamkha, A. J., & Ganji, D. D. (2020). Natural convection analysis in a square enclosure with a wavy circular heater under magnetic field and nanoparticles. *Journal of Thermal Analysis and Calorimetry*, 139(1), 661–671. <https://doi.org/10.1007/s10973-019-08408-0>
- Du, B. C., He, Y. L., Wang, K., & Zhu, H. H. (2017). Convective heat transfer of molten salt in the shell-and-tube heat exchanger with segmental baffles. *International Journal of Heat and Mass Transfer*, 113, 456–465. <https://doi.org/10.1016/j.ijheatmasstransfer.2017.05.075>
- Eiamsa-ard, S., & Chuwattanakul, V. (2020). Visualization of heat transfer characteristics using thermochromic liquid crystal temperature measurements in channels with inclined and transverse twisted-baffles. *International Journal of Thermal Sciences*, 153, 106358. <https://doi.org/10.1016/j.ijthermalsci.2020.106358>
- Ekiciler, R. (2020). Effects of novel hybrid nanofluid (TiO₂-Cu/EG) and geometrical parameters of triangular rib mounted in a duct on heat transfer and flow characteristics. *Journal of Thermal Analysis and Calorimetry*. <https://doi.org/10.1007/s10973-020-09913-3>
- Endres, L. A. M., & Möller, S. V. (2001). On the fluctuating wall pressure field in tube banks. *Nuclear Engineering and Design*, 203(1), 13–26. [https://doi.org/10.1016/S0029-5493\(00\)00293-4](https://doi.org/10.1016/S0029-5493(00)00293-4)
- Gao, T., Zhu, J., Li, J., & Xia, Q. (2018). Numerical study of the influence of rib orientation on heat transfer enhancement

- in two-pass ribbed rectangular channel. *Engineering Applications of Computational Fluid Mechanics*, 12(1), 117–136. <https://doi.org/10.1080/19942060.2017.1360210>
- Ghalandari, M., Bornassi, S., Shamshirband, S., Mosavi, A., & Chau, K. W. (2019). Investigation of submerged structures' flexibility on sloshing frequency using a boundary element method and finite element analysis. *Engineering Applications of Computational Fluid Mechanics*, 13(1), 519–528. <https://doi.org/10.1080/19942060.2019.1619197>
- Gorla, R. S. R., & Chamkha, A. (2011). Natural convective boundary layer flow over a nonisothermal vertical plate embedded in a porous medium saturated with a nanofluid. *Nanoscale and Microscale Thermophysical Engineering*, 15(2), 81–94. <https://doi.org/10.1080/15567265.2010.549931>
- Hassan, H., & Abo-Elfadl, S. (2018). Experimental study on the performance of double pass and two inlet ports solar air heater (SAH) at different configurations of the absorber plate. *Renewable Energy*, 116(A), 728–740. <https://doi.org/10.1016/j.renene.2017.09.047>
- Ho, C. D., Hsiao, C. F., Chang, H., & Tien, Y. E. (2017). Investigation of device performance for recycling double-pass V-corrugated solar air collectors. *Energy Procedia*, 105, 28–34. <https://doi.org/10.1016/j.egypro.2017.03.275>
- Hoseinzadeh, S., Heyns, P. S., Chamkha, A. J., & Shirkhani, A. (2019). Thermal analysis of porous fins enclosure with the comparison of analytical and numerical methods. *Journal of Thermal Analysis and Calorimetry*, 138(1), 727–735. <https://doi.org/10.1007/s10973-019-08203-x>
- Jain, S. K., Agrawal, G. D., & Misra, R. (2019). A detailed review on various V-shaped ribs roughened solar air heater. *Heat and Mass Transfer*, 55(12), 3369–3412. <https://doi.org/10.1007/s00231-019-02656-4>
- Jayavel, S., & Tiwari, S. (2010). Finite volume algorithm to study the effect of tube separation in flow past channel confined tube banks. *Engineering Applications of Computational Fluid Mechanics*, 4(1), 39–57. <https://doi.org/10.1080/19942060.2010.11015298>
- Jedsadaratanachai, W., & Boonloi, A. (2014). Effects of blockage ratio and pitch ratio on thermal performance in a square channel with 30° double V-baffles. *Case Studies in Thermal Engineering*, 4, 118–128. <https://doi.org/10.1016/j.csite.2014.08.002>
- Kabeel, A. E., Hamed, M. H., Omar, Z. M., & Kandeal, A. W. (2018). Influence of fin height on the performance of a glazed and bladed entrance single-pass solar air heater. *Solar Energy*, 162, 410–419. <https://doi.org/10.1016/j.solener.2018.01.037>
- Kumar, A., & Kim, M. H. (2015). Convective heat transfer enhancement in solar air channels. *Applied Thermal Engineering*, 89, 239–261. <https://doi.org/10.1016/j.applthermaleng.2015.06.015>
- Kumar, K., Prajapati, D. R., & Samir, S. (2018). Heat transfer and friction characteristics of artificially roughened duct used for solar air heaters—A review. *Journal of The Institution of Engineers (India): Series C*, 99(1), 105–123. <https://doi.org/10.1007/s40032-017-0415-5>
- Kumar, K. G., Rahimi-Gorji, M., Reddy, M. G., Chamkha, A. J., & Alarif, I. M. (2020). Enhancement of heat transfer in a convergent/divergent channel by using carbon nanotubes in the presence of a Darcy-Forchheimer medium. *Microsystem Technologies*, 26(2), 323–332. <https://doi.org/10.1007/s00542-019-04489-x>
- Lauder, B. E., & Spalding, D. B. (1974). The numerical computation of turbulent flows. *Computer Methods in Applied Mechanics and Engineering*, 3(2), 269–289. [https://doi.org/10.1016/0045-7825\(74\)90029-2](https://doi.org/10.1016/0045-7825(74)90029-2)
- Lei, Y. G., He, Y. L., Li, R., & Gao, Y. F. (2008). Effects of baffle inclination angle on flow and heat transfer of a heat exchanger with helical baffles. *Chemical Engineering and Processing: Process Intensification*, 47(12), 2336–2345. <https://doi.org/10.1016/j.cep.2008.01.012>
- Leonard, B. P., & Mokhtari, S. (1990). ULTRA-SHARP nonoscillatory convection schemes for high-speed steady multidimensional flow.
- Liang, Y., Liu, P., Zheng, N., Shan, F., Liu, Z., & Liu, W. (2019). Numerical investigation of heat transfer and flow characteristics of laminar flow in a tube with center-tapered wavy-tape insert. *Applied Thermal Engineering*, 148, 557–567. <https://doi.org/10.1016/j.applthermaleng.2018.11.090>
- Mehryan, S. A. M., Izadpanahi, E., Ghalambaz, M., & Chamkha, A. J. (2019). Mixed convection flow caused by an oscillating cylinder in a square cavity filled with Cu-Al₂O₃/water hybrid nanofluid. *Journal of Thermal Analysis and Calorimetry*, 137(3), 965–982. <https://doi.org/10.1007/s10973-019-08012-2>
- Menni, Y., & Azzi, A. (2018). Design and performance evaluation of air solar channels with diverse baffle structures. *Computational Thermal Sciences: An International Journal*, 10(3), 225–249. <https://doi.org/10.1615/ComputThermalScien.2018025026>
- Menni, Y., Azzi, A., & Chamkha, A. J. (2019). Computational thermal analysis of turbulent forced-convection flow in an air channel with a flat rectangular fin and downstream V-shaped baffle. *Heat Transfer Research*, 50(18), 1781–1818. <https://doi.org/10.1615/HeatTransRes.2019026143>
- Menni, Y., Azzi, A., Didi, F., & Harmand, S. (2018). Computational fluid dynamical analysis of new obstacle design and its impact on the heat transfer enhancement in a specific type of air flow geometry. *Computational Thermal Sciences: An International Journal*, 10(5), 421–447. <https://doi.org/10.1615/ComputThermalScien.2018024416>
- Menni, Y., Azzi, A., & Zidani, C. (2018). CFD simulation of thermo-aeraulic fields in a channel with multiple baffle plates. *Journal of Thermal Engineering*, 4(6), 2481–2495. <https://doi.org/10.18186/thermal.465696>
- Mohebbi, R., Izadi, M., & Chamkha, A. J. (2017). Heat source location and natural convection in a C-shaped enclosure saturated by a nanofluid. *Physics of Fluids*, 29(12), 122009. <https://doi.org/10.1063/1.4993866>
- Nakhchi, M. E., Esfahani, J. A., & Kim, K. C. (2020). Numerical study of turbulent flow inside heat exchangers using perforated louvered strip inserts. *International Journal of Heat and Mass Transfer*, 148, 119143. <https://doi.org/10.1016/j.ijheatmasstransfer.2019.119143>
- Nasiruddin, S., & Siddiqui, M. H. K. (2007). Heat transfer augmentation in a heat exchanger tube using a baffle. *International Journal of Heat and Fluid Flow*, 28(2), 318–328. <https://doi.org/10.1016/j.ijheatfluidflow.2006.03.020>
- Patankar, S. V. (1980). *Numerical heat transfer and fluid flow*. McGraw-Hill.

- Petukhov, B. S. (1970). Heat transfer and friction in turbulent pipe flow with variable physical properties. *Advances in Heat Transfer*, 6, 503–564. [https://doi.org/10.1016/S0065-2717\(08\)70153-9](https://doi.org/10.1016/S0065-2717(08)70153-9)
- Pourramezan, M., Ajam, H., Raoufi, M. A., & Abadeh, A. (2020). Performance evaluation and optimization of design parameters for twisted conical strip inserts in tubular laminar flow using Taguchi approach. *International Journal of Thermal Sciences*, 152, 106324. <https://doi.org/10.1016/j.ijthermalsci.2020.106324>
- Promvong, P., & Skullong, S. (2019a). Heat transfer augmentation in solar receiver heat exchanger with hole-punched wings. *Applied Thermal Engineering*, 155, 59–69. <https://doi.org/10.1016/j.applthermaleng.2019.03.132>
- Promvong, P., & Skullong, S. (2019b). Heat transfer in solar receiver heat exchanger with combined punched-V-ribs and chamfer-V-grooves. *International Journal of Heat and Mass Transfer*, 143, 118486. <https://doi.org/10.1016/j.ijheatmasstransfer.2019.118486>
- Promvong, P., & Skullong, S. (2020). Augmented heat transfer in tubular heat exchanger fitted with V-baffled tape. *International Journal of Thermal Sciences*, 155, 106429. <https://doi.org/10.1016/j.ijthermalsci.2020.106429>
- Promvong, P., Tamna, S., Pimsarn, M., & Thianpong, C. (2015). Thermal characterization in a circular tube fitted with inclined horseshoe baffles. *Applied Thermal Engineering*, 75, 1147–1155. <https://doi.org/10.1016/j.applthermaleng.2014.10.045>
- Promvong, P., & Thianpong, C. (2008). Thermal performance assessment of turbulent channel flows over different shaped ribs. *International Communications in Heat and Mass Transfer*, 35(10), 1327–1334. <https://doi.org/10.1016/j.icheatmasstransfer.2008.07.016>
- Reddy, K. S., & Satyanarayana, G. V. (2008). Numerical study of porous finned receiver for solar parabolic trough concentrator. *Engineering Applications of Computational Fluid Mechanics*, 2(2), 172–184. <https://doi.org/10.1080/19942060.2008.11015219>
- Saini, S. K., & Saini, R. P. (2008). Development of correlations for Nusselt number and friction factor for solar air heater with roughened duct having arc-shaped wire as artificial roughness. *Solar Energy*, 82(12), 1118–1130. <https://doi.org/10.1016/j.solener.2008.05.010>
- Saleh, H., Siri, Z., & Hashim, I. (2019). Role of fluid-structure interaction in mixed convection from a circular cylinder in a square enclosure with double flexible oscillating fins. *International Journal of Mechanical Sciences*, 161–162, 105080. <https://doi.org/10.1016/j.ijmecsci.2019.105080>
- Salih, S. Q., Aldlemy, M. S., Rasani, M. R., Ariffin, A. K., Ya, T. M. Y. S. T., Al-Ansari, N., Yaseen, Z. M., & Chau, K. W. (2019). Thin and sharp edges bodies-fluid interaction simulation using cut-cell immersed boundary method. *Engineering Applications of Computational Fluid Mechanics*, 13(1), 860–877. <https://doi.org/10.1080/19942060.2019.1652209>
- Samadianfard, S., Majnooni-Heris, A., Qasem, S. N., Kisi, O., Shamshirband, S., & Chau, K. (2019). Daily global solar radiation modeling using data-driven techniques and empirical equations in a semi-arid climate. *Engineering Applications of Computational Fluid Mechanics*, 13(1), 142–157. <https://doi.org/10.1080/19942060.2018.1560364>
- Saravanakumar, P. T., Somasundaram, D., & Matheswaran, M. M. (2020). Exergetic investigation and optimization of arc shaped rib roughened solar air heater integrated with fins and baffles. *Applied Thermal Engineering*. <https://doi.org/10.1016/j.applthermaleng.2020.115316>
- Singh, S., Chander, S., & Saini, J. S. (2011). Heat transfer and friction factor correlations of solar air heater ducts artificially roughened with discrete V-down ribs. *Energy*, 36(8), 5053–5064. <https://doi.org/10.1016/j.energy.2011.05.052>
- Skullong, S., Kwankaomeng, S., Thianpong, C., & Promvong, P. (2014). Thermal performance of turbulent flow in a solar air heater channel with rib-groove turbulators. *International Communications in Heat and Mass Transfer*, 50, 34–43. <https://doi.org/10.1016/j.icheatmasstransfer.2013.11.001>
- Skullong, S., Thianpong, C., Jayranaiwachira, N., & Promvong, P. (2016). Experimental and numerical heat transfer investigation in turbulent square-duct flow through oblique horseshoe baffles. *Chemical Engineering and Processing: Process Intensification*, 99, 58–71. <https://doi.org/10.1016/j.ccep.2015.11.008>
- Sripattanapipat, S., & Promvong, P. (2009). Numerical analysis of laminar heat transfer in a channel with diamond-shaped baffles. *International Communications in Heat and Mass Transfer*, 36(1), 32–38. <https://doi.org/10.1016/j.icheatmasstransfer.2008.09.008>
- Sriromreun, P., Thianpong, C., & Promvong, P. (2012). Experimental and numerical study on heat transfer enhancement in a channel with Z-shaped baffles. *International Communications in Heat and Mass Transfer*, 39(7), 945–952. <https://doi.org/10.1016/j.icheatmasstransfer.2012.05.016>
- Takhar, H. S., Chamkha, A. J., & Nath, G. (2001). Unsteady three-dimensional MHD-boundary-layer flow due to the impulsive motion of a stretching surface. *Acta Mechanica*, 146(1–2), 59–71. <https://doi.org/10.1007/BF01178795>
- Torii, K., Kwak, K. M., & Nishino, K. (2002). Heat transfer enhancement accompanying pressure-loss reduction with winglet-type vortex generators for fin-tube heat exchangers. *International Journal of Heat and Mass Transfer*, 45(18), 3795–3801. [https://doi.org/10.1016/S0017-9310\(02\)00080-7](https://doi.org/10.1016/S0017-9310(02)00080-7)
- Vatani, A., & Mohammed, H. A. (2013). Turbulent nanofluid flow over periodic rib-grooved channels. *Engineering Applications of Computational Fluid Mechanics*, 7(3), 369–381. <https://doi.org/10.1080/19942060.2013.11015478>
- Wang, F., Zhang, J., & Wang, S. (2012). Investigation on flow and heat transfer characteristics in rectangular channel with drop-shaped pin fins. *Propulsion and Power Research*, 1(1), 64–70. <https://doi.org/10.1016/j.jprr.2012.10.003>
- Wen, J., Yang, H., Wang, S., Xue, Y., & Tong, X. (2015). Experimental investigation on performance comparison for shell-and-tube heat exchangers with different baffles. *International Journal of Heat and Mass Transfer*, 84, 990–997. <https://doi.org/10.1016/j.ijheatmasstransfer.2014.12.071>
- Xu, S., Guo, Z., Hu, G., Chen, W., Lewis, R., & Wong, C. N. (2014). Thermal and flow fields in single board computer cabin systems using CFD analysis. *Engineering Applications of Computational Fluid Mechanics*, 8(4), 574–585. <https://doi.org/10.1080/19942060.2014.11083308>
- Yu, C., Zhang, H., Zeng, M., Wang, R., & Gao, B. (2020). Numerical study on turbulent heat transfer performance of a new compound parallel flow shell and tube heat exchanger

- with longitudinal vortex generator. *Applied Thermal Engineering*, 164, 114449. <https://doi.org/10.1016/j.applthermaleng.2019.114449>
- Zaraki, A., Ghalambaz, M., Chamkha, A. J., Ghalambaz, M., & De Rossi, D. (2015). Theoretical analysis of natural convection boundary layer heat and mass transfer of nanofluids: Effects of size, shape and type of nanoparticles, type of base fluid and working temperature. *Advanced Powder Technology*, 26(3), 935–946. <https://doi.org/10.1016/j.apt.2015.03.012>
- Zhang, L., Yan, X., Zhang, Y., Feng, Y., Li, Y., Meng, H., Zhang, J., & Wu, J. (2019). Heat transfer enhancement by streamlined winglet pair vortex generators for helical channel with rectangular cross section. *Chemical Engineering and Processing: Process Intensification*. <https://doi.org/10.1016/j.cep.2019.107788>
- Zhou, G., & Ye, Q. (2012). Experimental investigations of thermal and flow characteristics of curved trapezoidal winglet type vortex generators. *Applied Thermal Engineering*, 37, 241–248. <https://doi.org/10.1016/j.applthermaleng.2011.11.024>